Mathematical Modelling and Numerical Simulation with Applications, 2024, 4(5), 6–44

https://dergipark.org.tr/en/pub/mmnsa
ISSN Online: 2791-8564 / Open Access
https://doi.org/10.53391/mmnsa.1545438

RESEARCH PAPER

A non-linear diffusion problem with power-law diffusivity: An approximate solution experimenting with a modified sinc function

Jordan Hristov [1,*,‡]

[1]Department of Chemical Engineering, University of Chemical Technology and Metallurgy, Sofia 1756, Bulgaria

* Corresponding Author
‡ jordan.hristov@mail.bg, jyh@uctm.edu (Jordan Hristov)

Abstract

Employing a modified version of the cardinal $Sinc_\pi\left(\pi x^n\right)$ function as the assumed profile, the work presents approximate solutions of a non-linear (degenerate) diffusion equation with a power-law-type concentration-dependent diffusivity in a semi-infinite domain by the integral-balance method (double integration technique). The behavior and basic features of a modified function $Sinc_\pi\left(x^n\right)$ are addressed, highlighting how it is used in the generated approximate solutions. It has been successful in implementing the concept of the modified $sinc(x)$ function's variable (argument-dependent) exponent. To demonstrate the suitability of the suggested technique, comparative examinations concerning well-known approximate analytical and numerical problem solutions have been developed.

Keywords: Transient diffusion; approximate solutions; integral-balance method; sinc function

AMS 2020 Classification: 60J60; 70R50; 92F05; 97M50

1 Introduction

Approximate integral-balance solutions to parabolic diffusion models are based on the concept of Goodman [1] about the final penetration depth of the diffusant, resulting in a sharp front of the solution propagation [2–5]. It was extensively investigated for years and applied to solutions of practically important problems [6–14]. The essence of this method is the selection of an appropriate assumed profile and re-definition of the boundary conditions at the solution front (the so-called Goodman's boundary conditions; see Eq. (9) in Section 2). We do not intend to encompass all works where this powerful solution method is applied, and for this, we refer to the above-mentioned references (and the references therein) for more details (also in some additional literature sources quoted in the sequel of this article).

➤ **Received:** 08.09.2024 ➤ **Revised:** 06.11.2024 ➤ **Accepted:** 25.11.2024 ➤ **Published:** 31.12.2024

This communication, relevant to the field of engineering mathematics, addresses an approximate solution of a temperature (concentration)-dependent thermal (mass) diffusion model

$$\frac{\partial \theta}{\partial t} = \frac{\partial}{\partial x}\left(a\left(\theta\right)\frac{\partial \theta}{\partial x}\right) \Rightarrow \frac{\partial \theta}{\partial t} = \frac{\partial}{\partial x}\left(a_0\theta^m\frac{\partial \theta}{\partial x}\right). \tag{1}$$

In the model (1) the temperature (concentration)-dependent diffusivity is a power-law function of a scaled temperature (concentration) $a = k\left(\theta\right)/\rho C_p = a_0\left(\theta/\theta_{ref}\right)^m$, $m > 0$ (or as $D = D_0\left(\theta/\theta_{ref}\right)^m$, $m > 0$ in the case of heat of mass diffusion, where D_0 is the temperature (concentration)-independent diffusivity) (see more details and comments about the model and its properties in [15] and references therein).

The model (1) is uniformly parabolic but degenerates for $\theta = 0$ [16, 17] and followed by solutions with finite speeds and sharp fronts pertinent to creeping flows [18, 19], non-linear heat conductivity (mass diffusion, too) [20], porous media filtration [21]. Many problems defined with various positive integer values m are analyzed in [15–17, 19] and the references therein.

We have now completed the initial remarks regarding the use of the integral-balance method to solve diffusion problems with non-linear (degenerate) parabolic equation modeling and started working on the problem we intend to develop. In general, the work under consideration involves the development of an approximate integral-balance solution to (1) with an assumed profile. More specifically, its modification $\mathrm{Sinc}_\pi(x^n)$ (Section 3) is employed, with details systematically presented in the sequel.

Motivation

The main motivation for this study is driven by some specific properties of the cardinal $\mathrm{sinc}(x)$ function, precisely its normalized version $\mathrm{sinc}_\pi(x)$ (see Section 2) that to a greater extent suggest its use as an assumed profile in the integral-balance solution developed. Saying in advance, the main idea and what the attractive features of $\mathrm{sinc}_\pi(x)$ are that $\mathrm{sinc}_\pi(0) = 1$ and $\mathrm{sinc}_\pi(1) = 0$ (as explained in Section 2) and it is a completely monotonic decaying function in the range $0 \leq x \leq 1$ that matches, in general, the behavior of the approximate solutions when expressed function through the parabolic profile with unspecified exponent and other approximate solutions (see Section 2).

Aim

The key aim of this study is the use of a modified $\mathrm{sinc}(x)$ function, mentioned further as $\mathrm{Sinc}_\pi(x^n)$, as an assumed profile in the integral-balance solution; precisely, some new features of this function (presented in Section 3) suggest its use in a solution to the non-linear diffusion model (1) as an example of the effective performance of the idea.

The focus of this study and the main concept developed

Before continuing, we would like to stress the principal points pertinent to approximate solutions of degenerate parabolic models (sometimes called concentration-dependent models), developed by the integral-balance method, among them:

- Techniques of the integral method applied to develop the approximate solution (see Section 2).
- Assumed profiles and characteristics of the approximate solution related to variations in the degrees of model degeneracy (the value of the exponent m) (see Section 2).
- Why the $\mathrm{sinc}(x)$ function and its modification, conceived here, are chosen to develop an

approximate solution by the integral-balance method (see Section 2).
- The main concept of the study addresses the application of a modified $\mathrm{Sinc}_\pi(x^n)$ function as an assumed profile in the integral-balance solution (see Section 4).
- As a step beyond the main concept a version of a modified $\mathrm{Sinc}_\pi(x^n)$ function with a variable exponent (dependent on the argument) is developed towards the approximate integral-balance solutions (see Section 6).
- Comparisons of the developed solution with others available in the literature (see Section 6 and Section 7).

Further text organization

For the sake of clarity, the techniques used in approximate solutions developed are briefly presented in Section 2 and Section 2 together with a necessary initial transform of the model (1) allowing them to be applied (Section 2).

The first and primary step in developing the new approximate solution is the explanation of the choice of a modified version of the $\mathrm{sinc}(x)$ function to be used as the assumed profile, comparing it with the commonly applicable parabolic profile (Section 2). The assumed profile and its basic properties are presented in Section 3. New solutions are developed in Section 4. Numerical experiments with the new solutions and qualitative assessments are developed in Section 5 with outcomes envisaging further steps in the solution refinement. Section 6 focuses on solution refinements in two directions: i) Minimization of the approximation errors through optimization of the exponent of the modified $\mathrm{Sinc}_\pi(x^n)$ function through minimization of norms of residual functions (see Section 6), and ii) Solution optimization through approximation error minimization applying the concept of an argument-dependent exponent of the modified $\mathrm{Sinc}_\pi(x^n)$ function (see Section 6). Comparisons of the new solution with others (on the same problem) available in literature are presented in Section 7. For a more concise organization of the text, all cumbersome expressions and auxiliary developments are summarized in the Appendix 9.

2 The necessary background of the new solution

Approximate solution by the integral-balance method

Now, we present briefly the integration techniques of the integral balance method, and for the sake of clarity, at this point, we will use the linear diffusion model with $m = 0$, that is, constant diffusivity, namely

$$\frac{\partial \theta}{\partial t} = a\frac{\partial^2 \theta}{\partial x^2}, \quad \theta(x,t) = 0, \quad t > 0. \tag{2}$$

Now, we will briefly outline two basic integration techniques of the integral-balance method.

Single-integration method

The single integration technique, known as the heat-balance integral method (HBIM) [1, 5] uses an integration of Eq. (2) from x to δ, namely

$$\frac{d}{dt}\int_0^\delta \theta(x,t)\,dx - \theta(\delta,t)\frac{d\delta}{dt} = \int_0^\delta a\frac{\partial^2\theta}{\partial x^2}dx \Rightarrow \frac{d}{dt}\int_0^\delta \theta(x,t)\,dx = -a\frac{\partial\theta}{\partial x}(0,t). \tag{3}$$

In a semi-infinite medium, the condition $\theta(x \to \infty, t) = 0$ is replaced by sharp front concept conditions [1]

$$\theta(\delta) = \frac{\partial \theta}{\partial x}(\delta) = 0. \tag{4}$$

Then, θ should be replaced in (3) by the assumed profile $\theta_a = \theta_a(x/\delta)$ as a function of the dimensionless ratio (distance) x/δ . This yields a differential equation concerning $\delta(t)$. The drawback of HBIM is that the gradient of the right-side of (3) *should be defined through the assumed profile (we will refer to this when the main in the solution approximation developed in this article is discussed)*. The Double Integration Method (DIM) [15] (especially when the Dirichlet problem is at issue) avoids this problem, and the integration technique is briefly presented next.

Double-integration method

With this approach, a double integration concerning the spatial coordinate and application of the Leibniz rules yield [15]

$$\int_0^\delta \int_x^\delta \frac{\partial \theta(x,t)}{\partial t} dx dx = \int_0^\delta \int_x^\delta a \frac{\partial^2 \theta(x,t)}{\partial x^2} dx dx \Rightarrow \frac{d}{dt} \int_0^\delta \int_x^\delta \theta(x,t) dx dx = a\theta(0,t). \tag{5}$$

Hence, the right-hand side of the integral relation is independent of the gradient $x = 0$ and depends on the boundary condition only. The case with $m \neq 0$ needs a preliminary recasting of the diffusion terms as explained next.

Double-integration method in the case when $m \neq 0$

In the case when $m \neq 0$ we may transform the diffusion term as [15]) as

$$a_0 \theta^m \frac{\partial \theta}{\partial x} = \frac{a_0}{m+1} \frac{\partial \theta^{m+1}}{\partial x}, \tag{6}$$

and this allows us to present the model (1) as

$$\frac{\partial \theta(x,t)}{\partial t} = \frac{a_0}{m+1} \frac{\partial \theta^{m+1}}{\partial x^2}. \tag{7}$$

Then, the application of (5) results in

$$\frac{d}{dt} \int_0^\delta \int_x^\delta \theta(x,t) dx dx = \frac{a}{m+1} \theta^{m+1}(0,t). \tag{8}$$

Classic polynomial and parabolic approximate profile

The common approach at the very beginning of the integral method application is the use of polynomial profiles of 2nd or 3rd order that, in general, led to predetermined error approximation [1]. An alternative approach that matches, to some extent, the polynomial ones is the use of a parabolic profile (9), namely

$$\theta_a = \theta_s \left(1 - \frac{x}{\delta}\right)^{n_p} = \theta_s (1 - X)^{n_p}, \quad 0 \leq x \leq \delta, \quad 0 \leq X = x/\delta \leq 1, \tag{9}$$

with either $n_p = 2$ or $n_p = 3$ [5] (the subscript p denotes *parabolic*).

This profile satisfies the Goodman boundary conditions (4). Represented by the dimensionless space coordinate $X = x/\delta$ all profiles, despite the value of the exponent n goes to zero at $X = 1$. This feature is especially important when comparing solutions developed by different methods to the integral-balance solutions as it was done in [15].

A special feature of the parabolic profile (9) is the fact that if $n_p > 1$ (see Figure 1-left panel) it generates concave distributions, while for $n_p < 1$ (See Figure 1-right panel) the generated distributions are convex [15]. The convex profiles are typical solutions of transient diffusion with power-law diffusivity [6, 15].

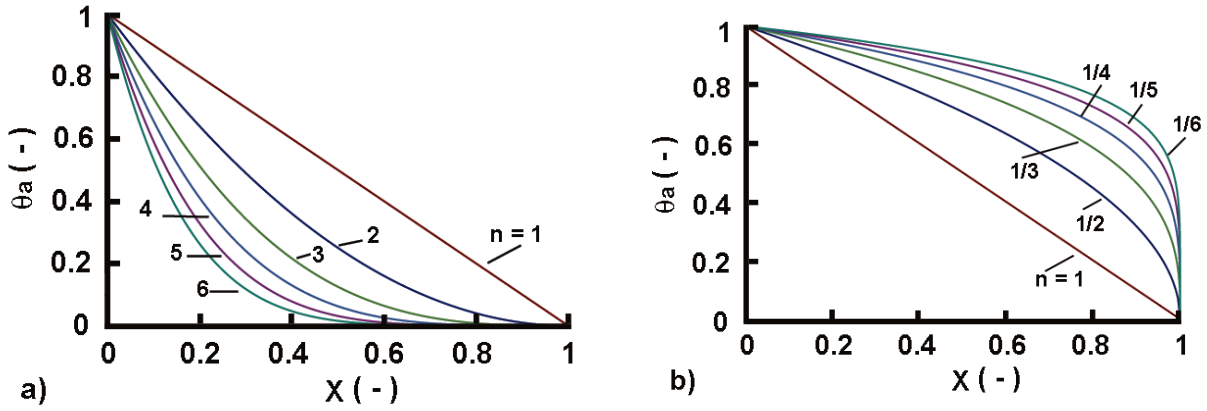

Figure 1. Parabolic profile (function) behavior controlled by values of the exponent n. a) Concave profiles generated for $n_p \geq 1$; b) Convex profiles generated for $n_p \leq 1$. Note: In b) the values of profile exponents are especially presented in the format $1/n$ for easy comparison with plots in panel a)

sinc(x) function

The non-normalized $\sin c\,(x) = \sin\,(x)/x$ function is defined as [22, 24, 25]

$$\operatorname{sinc}(x) = \begin{pmatrix} \dfrac{\sin(x)}{x},\ x \neq 0 \\ 1,\ x = 0 \end{pmatrix}, \tag{10}$$

while the normalized version is

$$\operatorname{sinc}_\pi(x) = \begin{pmatrix} \dfrac{\sin(\pi x)}{\pi x},\ x \neq 0 \\ 1,\ x = 0 \\ 0, x = 1 \end{pmatrix}, \tag{11}$$

$\operatorname{sinc}\,(x = 0) \sim \lim_{x\to 0} \frac{\sin(kx)}{kx} = 1$ for all real $k \neq 0$. Also, their integrals from $-\infty$ to ∞ are

$$\int_{-\infty}^{\infty} \frac{\sin(x)}{x} dx = \pi \Rightarrow \int_{0}^{\infty} \frac{\sin(x)}{x} dx = \frac{\pi}{2}, \quad \int_{-\infty}^{\infty} \frac{\sin(\pi x)}{\pi x} dx = 1 = \frac{1}{\pi} \int_{-\infty}^{\infty} \frac{\sin(x)}{x} dx. \tag{12}$$

The non-normalized *sinc* function $\mathrm{sinc}(x) = \sin(x)/x$ is defined for $x \neq 1$, while the normalized *sinc* function is $\sin c_\pi(x) = \sin(\pi x)/\pi x$. The normalized *sinc* function has a limit $\sin x(0) = 1$ for $x \to 0$. Moreover, $\mathrm{sinc}(x)$ and $\mathrm{sinc}_\pi(x)$ are analytical and entire functions [23]. The graphical representation is shown in Figure 2.

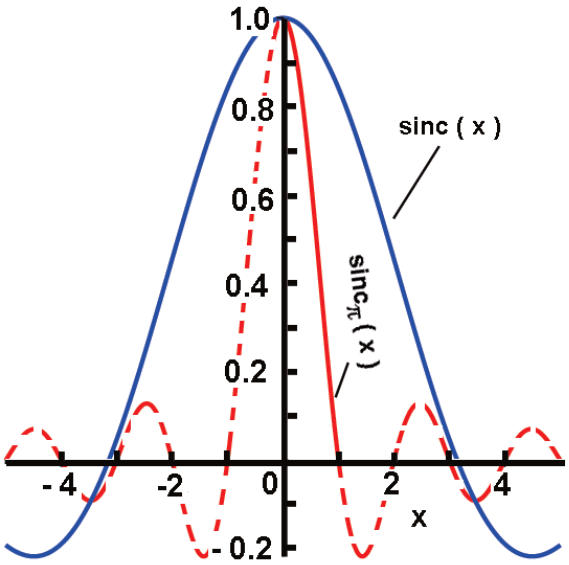

Figure 2. $sinc(x)$ (blue in the online version) and $sinc_\pi(\pi x)$ (red in the online version) behavior. We are interested in the non-oscillating branch of $sinc_\pi(\pi x)$ in the first quadrant (solid red line in the online version) for $0 \leq x \leq 1$

These versions are widely used in signal processing [26], mechanics of materials [27], Fourier transforms [28] and analysis [32], wavelet transforms [33] non-local operator formulations [33–38], numerical methods [29, 30], dielectric electromagnetic behavior through fractional (with singular kernel) modeling [31], etc. There is a vast work on the properties of both versions of the $\sin c(x)$ function, but now we refer to only what is needed to develop the approximate solution of the non-linear diffusion model (1).

An additional feature of the *sinc* function (that will be used further in this article) is the Taylor series expansion as [39]

$$\mathrm{sinc}(x) = \frac{\sin(x)}{x} = \sum_{k=0}^{\infty} \frac{(-1)^k (x^2)^k}{(2k+1)!} = 1 - \frac{x^2}{3!} + \frac{x^4}{5!} - \frac{x^6}{7!} + \ldots + |0|^{11}, \tag{13}$$

converging for all x.

Consequently, for the normalized version we have

$$\mathrm{sinc}(x) = \frac{\sin(\pi x)}{\pi x} = \sum_{k=0}^{\infty} \frac{(-1)^k (\pi x)^{2k}}{(2k+1)!} = 1 - \frac{(\pi x)^2}{3!} + \frac{(\pi x)^4}{5!} - \frac{(\pi x)^6}{7!} + \ldots + |0|^{11}. \tag{14}$$

Also, the *sinc* function can be represented through the Gamma function using Euler's reflection formula (15)

$$\mathrm{sinc}_\pi(x) = \frac{\sin(\pi x)}{\pi x} = \frac{1}{\Gamma(1+x)\,\Gamma(1-x)}. \tag{15}$$

The derivative of $\sin c\,(x)$ is

$$\sin c'\,(x)=\begin{cases}\dfrac{x\cos x-\sin x}{x^2}=\dfrac{\cos x-\sin cx}{x},\ x\neq 0\\ 0,\ x=0\end{cases}\qquad x\neq 0,\quad \sin c'\,(x=0)\to 0. \tag{16}$$

Hence, we have an undesirable singularity at $x=0$ since following the single integration method its relation (3) needs $\partial u_a\,(x=0)/\partial x$ to be defined through the assumed profile. Thus, the simple integration technique (HBIM) is inapplicable with the suggested modification $Sinc_\pi(\pi x^n)$ as assumed profile (see Section 3 and Section 4), and consequently, this invokes directly the Double Integration Method (DIM) since at $x=0$ we have to know only the boundary condition. Moreover, since $\sin c'\,(x=0)\to 0$ we cannot apply this assumed profile to the Neumann problem; this is a natural restriction coming from the assumed profile that does not stop the development of the problem considered here.

3 Modified $Sinc_\pi(x^n)$ function: definition and properties

The attractive feature of the *sinc* function, especially for the solutions developed in this work, is that it crosses the abscissa at $x=1$, a feature already demonstrated by the parabolic profile (9) when expressed in terms of $X=x/\delta\,(t)$. Reasonably, as it follows from the required approximation solution of the diffusion model we are interested only in the branch (non-oscillating section) of $Sinc_\pi(x^n)$ for $0\leq x\leq 1$. For the approximate solution developed next, we introduce a modified version $Sinc_\pi\,(x^n)$, defined as

$$Sinc_\pi\,(x^n)=\frac{\sin\,(\pi x^n)}{\pi x^n},\quad n>0,\quad 0\leq x\leq 1. \tag{17}$$

Similar to the expansion (14) we have (denoting for the sake of clarity $y=x^n$)

$$\sin c_\pi\,(x^n)=\frac{\sin\,(\pi y)}{\pi y}=\sum_{k=0}^{\infty}\frac{(-1)^k(\pi y)^{2k}}{(2k+1)!}=1-\frac{(\pi y)^2}{3!}+\frac{(\pi y)^4}{5!}-\frac{(\pi y)^6}{7!}+\ldots+|0|^{11}. \tag{18}$$

The attractive feature of the newly defined normalized *sinc* function denoted here as $Sinc\,(x^n)$ is that we have again the limits $Sinc_\pi\,(x^n)_{(x=1)}=0$ and $Sinc_\pi\,(x^n)_{(x=0)}=1$. Simple numerical experiments reveal that the exponent n can change the shape of the profile from concave to convex (see Figure 3-left panel and Figure 3-right panel). The normalized *sinc* function defined by (17) is the same as that from the basic definition since by a simple change of variable $y=x^n$ we get $sinc_\pi\,(y)=\sin\,(\pi y)/\pi y$. However, the exponent n allows controlling how *fast* or *slow* the argument x^n will change when $0\leq x\leq 1$.

To a greater extent, the behavior of these profiles resembles those generated by the parabolic one with an unspecified exponent (Section 2). Therefore, these features, mainly the possibility to generate simply convex profiles (as in Figure 3-left panel) raise your spirits to see what would be the integral-balance solutions when the assumed profile is defined by (17). Moreover, the elements of this function, because it operates within the range $0<x<1$ exhibit some features, pertinent to the above-mentioned behavior and they are explained next. The behavior of the $\mathrm{Sinc}_\pi\,(x^n)$ function, too attractive for the development of the present study, could be simply explained in a mechanistic manner as:

- Since $0<x<1$, then for $n>1$, we have $x<x^n$. In general, if there is a set of p exponents $n_1<n_2<n_3<\ldots<n_p$, then $x^{n_p}<\ldots<x^3<x^2<x$. Hence, with the increase in n , the

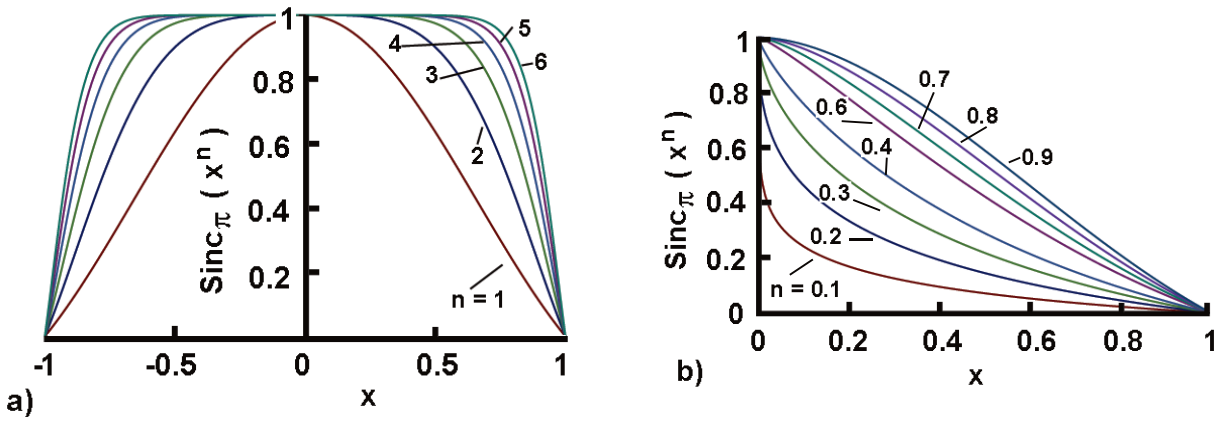

Figure 3. Profiles of $Sinc_\pi(x^n)$ function for two distinct sets of the exponent n within the range $0 \leq x \leq 1$. a) Convex profiles for $n > 1$ (we are interested in the behavior exhibited in the 1st quadrant only; b) Concave profiles for $n < 1$. See similar behaviors exhibited by the parabolic profiles in Figure 1

power x^n approaches a small value $x_0 \neq 0$ but very close to zero, i.e. represented as a limit this is $\lim_{n\to\infty} x^n \to 0$. In this context, we may see from (18) that for $n > 1$ and $0 < x < 1$ the series will converge more rapidly than in the case $n = 1$.

- At the same time, the behavior of $\sin(x^n)$ follows similarly, i.e. $\lim_{n\to\infty} \sin(x^n) \to 0$. Therefore, we have that $\lim_{n\to\infty} \mathrm{Sinc}_\pi(x^n) = \lim_{n\to\infty} [\sin(\pi x^n)/\pi x^n] \to 1$, because in this limit $n \to \infty$ is equivalent to $(\pi x^n) \to 0$. Since this is a theoretical limit that never will be reached, the practical behavior is $\lim_{n\to n_p} \mathrm{Sinc}_\pi(x^n) \to S_{n_p} < 1$ (S_{n_p}-a realistic limit of the function, at high values of n, but values of order of unity). Graphically, this means almost flat plots, with low negative trends located below the limit line 1 (see Figure 3-left panel).
- However, with the same domain $0 < x < 1$, the nominator $\sin(\pi x^n)$ exhibits *a strong negative skew* of the plots (i.e. a strong asymmetry with increase in the exponent n) with a trend toward a steep "'front shape"' for $x \to 1$, and finally, when x is close to the upper limit of the interval, this results in the steep front section of $\mathrm{Sinc}_\pi(x^n)$. This behavior is presented in Figure 4. **Note**: in terms of distributions (in statistics) we got a *left-skewed distribution* appearing as a *right-leaning curve*.

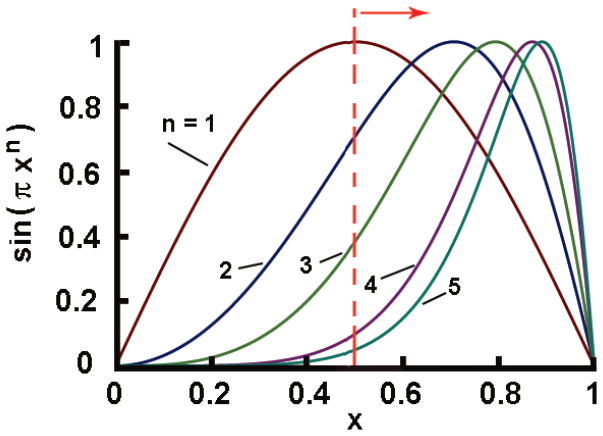

Figure 4. $Sinc_\pi(\pi x^n)$ behavior for various values of the exponent n demonstrating its effect on the negative skew development

4 A new approximate solution

Definition of the assumed profile

Based on the commented behavior of (17) we suggest an approximate profile defined through the normalized sinc_π function, denoted as $\text{Sinc}_\pi(x^n)$, in the following form:

$$u_a = u_s \,\text{Sinc}_\pi\left[\pi\left(\frac{x}{\delta\,(t)}\right)^n\right] = u_s\frac{\sin\left(\pi X^n\right)}{\pi X^n}, \quad 0 \le X = x/\delta \ \le 1, \tag{19}$$

where $u_s = u_a\,(x=0)$ because for $x = 0 \Rightarrow x/\delta(t) = X = 0$, and $sinc_{\pi X^n} = 1$.
This profile satisfies the Goodman conditions (4) because for $x = \delta(t) \Rightarrow X = x/\delta(t) = 1$ and $\text{Sinc}_\pi(\pi X^n) = d(\text{Sinc}_\pi(\pi X^n)/dX = 0$.

DIM solution:Dirichlet problem

The double-integration step

Consider a semi-infinite medium with a Dirichlet boundary condition to Eq. (1). With the assumed profile and the boundary condition at $x = 0$ we get $u_s = 1$. Then the integral balance relation of DIM (8) expressed through the dimensionless coordinate $X = x/\delta$ (as well as changing the variables and the terminals of the integrals) is

$$\frac{d\delta^2}{dt}\left[\int_0^1\left(\int_X^1\frac{\sin\left(\pi X^n\right)}{\pi X^n}dX\right)dX\right] = \frac{a_0}{m+1} \Rightarrow S_2\frac{d\delta^2}{dt} = \frac{a_0}{m+1}, \tag{20}$$

where

$$S_2\,(\pi, X) = \int_0^1\left(\int_X^1\frac{\sin\left(\pi X^n\right)}{\pi X^n}dX\right)dX, \quad 0 \le X = \frac{x}{\delta} \le 1. \tag{21}$$

The double integral in (21), denoted for brevity $S_2\,(\pi, X)$ is time-independent, and this step allows simply to solve (20) (taking into account the initial condition $\delta\,(t=0) = 0$) as

$$\delta = \sqrt{a_0 t}\sqrt{\frac{s_2}{m+1}}, \quad s_2 = 1/S_2. \tag{22}$$

Now, the primary problem is to evaluate $S_2\,(\pi, X)$. Since the direct integration of $S_2\,(\pi, X)$ is impossible we will use the expansion (14) expressed as a truncated series since it converges rapidly (for the sake of clarity see also the presentation (18))

$$S_2 = \int_0^1\left(\int_X^1\frac{\sin\left(\pi X^n\right)}{\pi X^n}dX\right)dX = \int_0^1\left(\int_X^1\sum_{k=0}^{K}\frac{(-1)^k(\pi X^n)^{2k}}{(2k+1)!}dX\right)dX, \quad 0 \le X = \frac{x}{\delta} \le 1. \tag{23}$$

The number of terms in the truncated series approximation

The series expansions of $\sin\left(\pi y\right)/\pi y$ converge rapidly as we can see directly next. For $n = 1$ in (23) we have as illustrative examples some cases with different numbers of terms of the truncated answers, namely:

For $K=3$,

$$S_2\left(K=3\right)=\frac{1}{2}-\frac{1}{24}\pi^2+\frac{1}{720}\pi^4-\frac{1}{40320}\pi^6\approx 0.20020\Rightarrow s_2\left(K=3\right)\approx 4.9950. \tag{24}$$

Similarly, for $K=5$

$$\begin{aligned} &S_2\left(K=5\right)=\frac{1}{2}-\frac{1}{24}\pi^2+\frac{1}{720}\pi^4-\frac{1}{40320}\pi^6+\frac{1}{3628800}\pi^8-\frac{1}{479001600}\pi^{10}\approx 0.20262\\ &\Rightarrow s_2\left(K=5\right)\approx 4.9353. \end{aligned} \tag{25}$$

That is $s_2\left(K=5\right)\approx 4.9353$.
For $K=10$ we have $S_2\left(K=10\right)\approx 0.20263$ and consequently $s_2\left(K=10\right)\approx 4.9351$. Hence, from a practical point of view, it is reasonable to use a truncated series for $K=10$, and this is consistent with the series expansions (13) and (14).
However, when $n\neq 1$ we get, as a first step of the approximation, a truncated series $S_1\left(K,n,X\right)$ defined through the first integration in (23), namely

$$\begin{aligned} S_1\left(K=3,n\right)&=\int_X^1\left(1-\frac{1}{6}\pi^2X^{2n}+\frac{1}{120}\pi^4X^{4n}-\frac{1}{5040}\pi^6X^{6n}\right)dX\\ &=\left[X-\frac{1}{6}\frac{\pi^2X^{2n+1}}{\left(2n+1\right)}+\frac{1}{120}\frac{\pi^4X^{4n+1}}{\left(4n+1\right)}-\frac{1}{5040}\frac{\pi^6X^{6n+1}}{\left(6n+1\right)}\right]\Big|_X^1. \end{aligned} \tag{26}$$

Then,the second integration in (23) leads to $S_2=\int_0^1 S_1dX$ as

$$\begin{aligned} S_2\left(K=3,n\right)&=\left(1-\frac{1}{6}\frac{\pi^2}{2n+1}+\frac{1}{120}\frac{\pi^4}{4n+1}-\frac{1}{5040}\frac{\pi^6}{6n+1}\right)\\ &-\left(\frac{1}{2}-\frac{1}{6}\frac{\pi^2}{\left(2n+1\right)\left(2n+2\right)}+\frac{1}{120}\frac{\pi^4}{\left(4n+1\right)\left(4n+2\right)}-\frac{1}{5040}\frac{\pi^6}{\left(6n+1\right)\left(6n+2\right)}\right). \end{aligned} \tag{27}$$

With the general series expression (14) we get

$$S_2=\int_0^1\left(\int_X^1\frac{\sin\left(\pi X^n\right)}{\pi X^n}dX\right)dX=\int_0^1\left(\int_X^1\sum_{k=0}^K\frac{\left(-1\right)^k\left(\pi X^n\right)^{2k}}{\left(2k+1\right)!}dX\right)dX. \tag{28}$$

Then the integration yields

$$\begin{aligned} S_2&=\int_0^1\left(\sum_{k=0}^K\frac{\left(-1\right)^k\pi^{2k}}{\left(2kn+1\right)\left(2k+1\right)!}\left(1-X^{2kn+1}\right)\right)dX=\sum_{k=0}^K\frac{\left(-1\right)^k\pi^{2k}}{\left(2kn+1\right)\left(2k+1\right)!}\int_0^1\left(1-\frac{X^{2kn+1}}{\left(2kn+1\right)}\right)dX\\ &=\sum_{k=0}^K\frac{\left(-1\right)^k\pi^{2k}}{\left(2kn+1\right)\left(2k+1\right)!}\left[1-\frac{1}{\left(2kn+1\right)\left(2kn+2\right)}\right]. \end{aligned} \tag{29}$$

Penetration depth and similarity variable

From (22) we see that both n and m control the penetration depth. It can be presented in a dimensionless form as

$$\frac{\delta(t)}{\sqrt{a_0 t}} = \sqrt{\frac{s_2}{m+1}} \Rightarrow \delta^2 = (a_0 t)\frac{s_2}{m+1} = (a_0 t)\frac{1}{S_2(m+1)}. \tag{30}$$

That is, with a stipulated value of n the increases in the non-linearity through m results in shorter penetration depths (this was already demonstrated in [15]), but we like to see other aspects of the relationship (30).

From the definition of $X = x/\delta(t)$ we have

$$X = \frac{x}{\sqrt{a_0 t}\sqrt{S_2(m+1)}} = \frac{\eta}{\sqrt{S_2(m+1)}}, \quad \eta = \frac{x}{\sqrt{a_0 t}}, \tag{31}$$

where $\eta = x/\sqrt{a_0 t}$ is the Boltzmann similarity variable that from (31) can be related to the generalized dimensionless variable X as $\eta = X\sqrt{S_2}(m+1)$.

Setting $X = 1$, whereby, the general definition, the assumed profile crosses the abscissa, we get the penetration depth, measured by η, where the profile will cross the abscissa, i.e. $\eta = \sqrt{S_2(m+1)}$. Then, we may plot the solution in terms of the similarity variable η varying the non-linear parameter m and the exponent n as shown in Figure 5 (see the next Section 5). Due to the nature of the $\mathrm{sinc}(x)$ plots, there are small oscillations after the point where the profiles cross the abscissa. However, as mentioned at the beginning, this section is outside the area of the approximate solutions. In terms of the the similarity variable η the approximate profile (19) can be expressed as

$$u_a = \frac{\sin\left(\pi\left(\frac{\eta}{\sqrt{S_2(m+1)}}\right)^n\right)}{\pi\left(\frac{\eta}{\sqrt{S_2(m+1)}}\right)^n}. \tag{32}$$

5 Numerical experiments

Qualitative numerical simulations of the approximate profiles

Approximate profiles in terms of the similarity variable η

It is evident from the plots in Figure 5 (top row) that the penetration depth shortens as m increases. When n is specified but m is variable, the same result is seen. This suggests that n and m have comparable impacts on the profiles, raising the obvious question of whether or not these exponents are related. The model determines the value of m, thus the only thing remaining to be done is to define n. Whether or not n is related to m, the solution to this question will be found in the sequel's parts. **Note**: Due to the nature of the $\mathrm{sinc}(x)$ plots, there are small oscillations after the points where the profiles cross the abscissa, but as mentioned at the beginning, these sections are outside the areas of the approximate solutions.

Approximate profiles in terms of the dimensionless variable X

Alternatively, when the approximate solution is expressed in terms of the dimensionless variable X, then the effect of n and m is not so obvious, but in general, with the increase in n the profiles become more rectangular and *vice versa*, as shown in Figure 6.

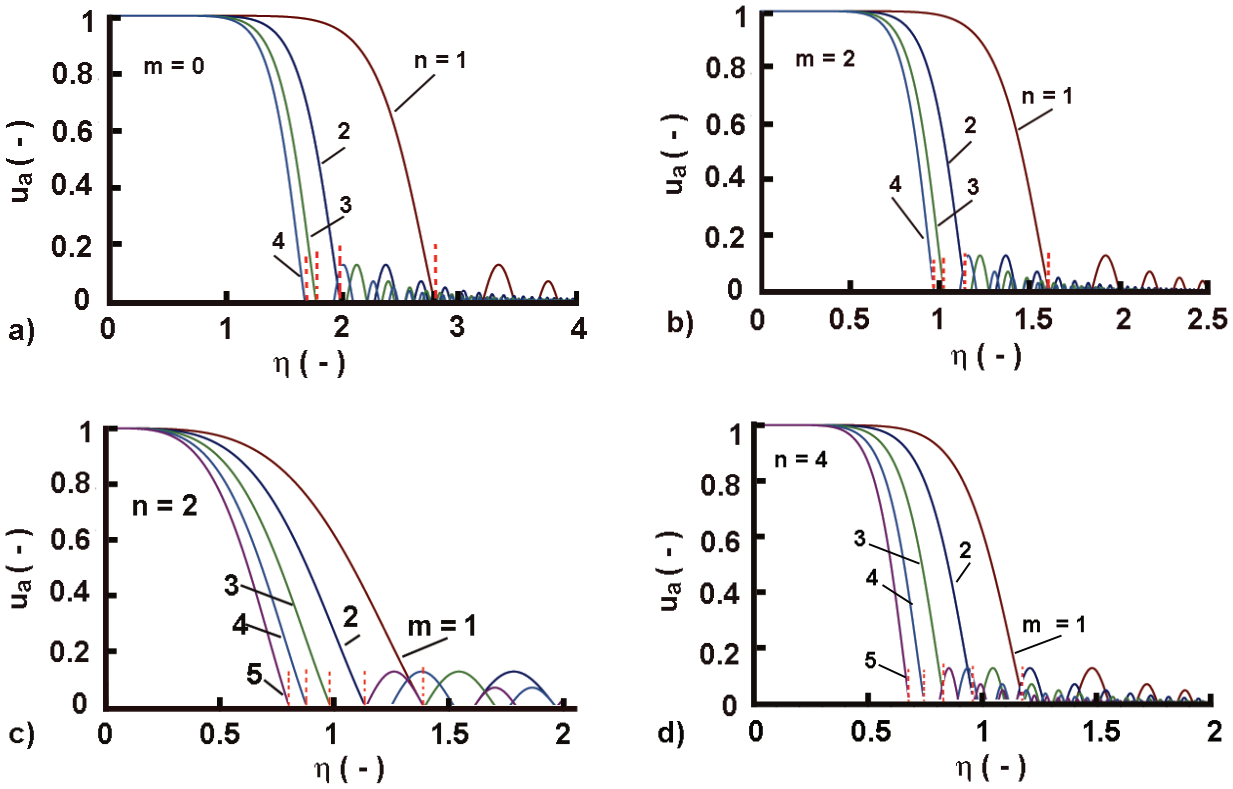

Figure 5. Qualitative plots of approximate solutions as functions of the similarity variable η for various values of the non-linear parameter m and with effects of exponent n on both the profile shape and the penetration depth. Upper row: a) and b) For a stipulated m and various n; Bottom row: c) and d) For a stipulated n and various m. Note: The vertical dashed lines (red in the online version) mark the penetration depths, measured in terms of the similarity variable η

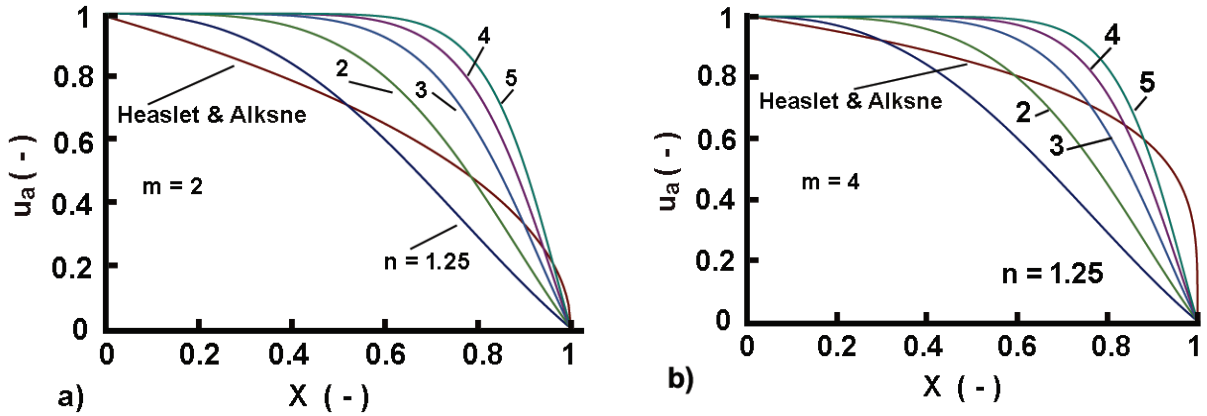

Figure 6. Qualitative plots of approximate solutions as functions of the dimensionless variable X for various values of the exponent n (see the effect on the profile shape). A comparison with the Heaslet and Alksne solution [40] (the red line in the online version)

Some briefs on the qualitative experiments

The presented qualitative numerical experiments reveal some basic features and related problems of the developed approximate solution, among them:

- In general, the approximate solution generates convex profiles with an increase in the value n that is in agreement with the general idea of this study when considering that between n and m, a functional relationship should be established.
- Second, since the non-linear diffusion model solved here has no exact solution, the solution of Heaslet and Alksne [40] and that developed by parabolic profiles [15], considered as correct solutions, are used for comparison. We see that the new solutions, without correct defined values of n, do not match, generally, the correct solutions as we would like. Explanations about these reference solutions are provided in the next Section 5).
- The behavior of the profile, with fixed (stipulated) values of n intuitively leads to the idea that it should depend to a greater extent on the variable X such as: for high values of X when $X \to 1$ the exponent n should increase thus allowing to creation of the steep front of the profile. For $X \to 0$ we need no so flat profiles that would be obtained if n will increase with the increase in X (this idea is developed in Section 6).

On the reference solutions used

Now, it is mandatory to define the reference solutions used further in this work for benchmarking the new results. In this context, two commonly used approximate solutions to (1) are briefly explained next.

The current solution, as previously done in Section 5, was qualitatively compared to Heaslet and Alksne's series solution [40] (see Figure 6). The rationale for this was because the Eq. (1) belongs to a family of non-linear models, to which all approximate solutions available have been compared (benchmarked) utilizing the result of [40] (see some comments in this direction in Section 7). This solution also makes use of the idea of a finite depth, which is identified in the original study, in the context of the following analysis of this research, as η_F (the analog of δ used here). The series then addresses the normalized variable $X = \eta/\eta_F$ ($\eta = x/\sqrt{a_0 t}$ is the similarity Boltzmann variable); in the case of integral-balance solutions η_F corresponds to $\sqrt{S_2\,(m+1)}$ in (32) because for $\eta = \sqrt{S_2\,(m+1)}$ we have $X = 1$. Section 7 also has some briefs on this solution. It is worth noting, that Heaslet and Alksne's solution explores cases with an upper limit of the exponent $m = 4$; the present work also matches this range but goes beyond up to $m \approx 10$. Thus, benchmarking Heaslet and Alksne's solutions, for $m > 4$, used further in this work, are generated by implementing their algorithm in Maple.

The second reference solution is based on the parabolic profile (9) explained in Section 2 and DIM solution (5), and developed in detail in [15]. As was proved in [15] it can succeed in approaching the Heaslet and Alksne's solution with an absolute error of less than 0.02.

Thus, we have two available approximate solutions (since (1) has no exact solution) allowing us to see what the concept is to use the modified $Sinc_\pi\,(\pi X^n)$ function as an assumed profile in the integral-balance solution.

6 Solution refinements

The solution refinement has only one task: to minimize the approximation error through the definition (determination) of the optimal value of the exponent n. In what follows we will explore two approaches:

- Minimization of the residual function over the range $0 \le X \le 1$ with the assumption $n = const.$, as the basic solution was done (Section 6).
- Looking for a suitable functional relationship $n = f(X)$, an approach mainly driven by intuition and preceding experience in optimization of integral-balance solutions [41] (Section 6).

Residual function minimization with constant exponent n

When the solution of the model (1) differs from the exact one, if any, then the residual function defined as (33) (all cumbersome expressions used in the remainder of this section are summarized in the Appendices) should attain its minimum over the domain $0 \leq X \leq 1$

$$R = \frac{\partial}{\partial t} Y\left(X^n\right) - \frac{a_0}{m+1} \frac{\partial^2}{\partial x^2} \left[Y\left(X^n\right)\right]^{m+1} \rightarrow \min . \tag{33}$$

In terms of the developed approximate solution, it can be presented as (see the development in Section 9 of the Appendix).

$$R = \frac{1}{t}\left\{\frac{1}{2}\frac{dY\left(X^n\right)}{dX} n X^n - S_2\left(m+1\right)\frac{\partial^2}{\partial X^2}\left[Y\left(X^n\right)\right]^{m+1}\right\} = \frac{1}{t} r\left(n, m, X\right), \tag{34}$$

where $Y\left(X\right) = Sinc_{\pi}\left(\pi X^n\right) = \sum\limits_{k=0}^{N} \frac{(-1)^k \pi^{2k}}{(2k+1)!} X^{2kn}$. Detailed expressions of the derivatives used in (34) are available in the Appendix (Section 9).

The residual function decays in time and therefore the optimization procedure should address the time-independent term $r\left(n, m, X\right)$. We need $r\left(n, m, X\right) \rightarrow \min$ over the interval $0 \leq X \leq 1$ because for $X = 0$ and $X = 1$ we have $R = 0$, taking into account that $Y\left(1\right) = 0$ and $Y\left(0\right) = 1 \rightarrow dY\left(0\right)/dX \ = 0$. Similar minimization techniques with parabolic assumed profiles may be found in [15].

Approximation errors through minimization of norms

We address two options to minimize the approximation error by applying two norms of the residual function, integrating them over the interval $0 \leq X \leq 1$, namely

$$E_{R_{L1}} = \int_0^1 R_{L1} dX = \int_0^1 |R| dX = \frac{1}{t}\int_0^1 |r| dX \Rightarrow e_{L1} = \int_0^1 |r| dX \rightarrow \min, \tag{35}$$

and

$$E_{R_{L2}} = \int_0^1 R_{L2} dX = \int_0^1 R^2 dX = \frac{1}{t^2}\int_0^1 r^2 dX \Rightarrow e_{L2} = \int_0^1 r^2 dX \rightarrow \min . \tag{36}$$

The optimization procedures were performed through Maple (such a subroutine exists in this computer algebra software) and additional numerical simulations adjusting the optimal values of the exponent n. The results are presented next.

Optimal n through minimization of L_1

This approach yields plots presented in Figure 7 and approximations compared to reference solutions in Figure 8. In general, the discrepancies between the approximate solutions and the reference ones of Heaslet and Alksne [40] and the parabolic profile-based [15] indicate the integral-balance solutions of the model (1) with optimal exponents defined through minimization of L_1 are unacceptable.

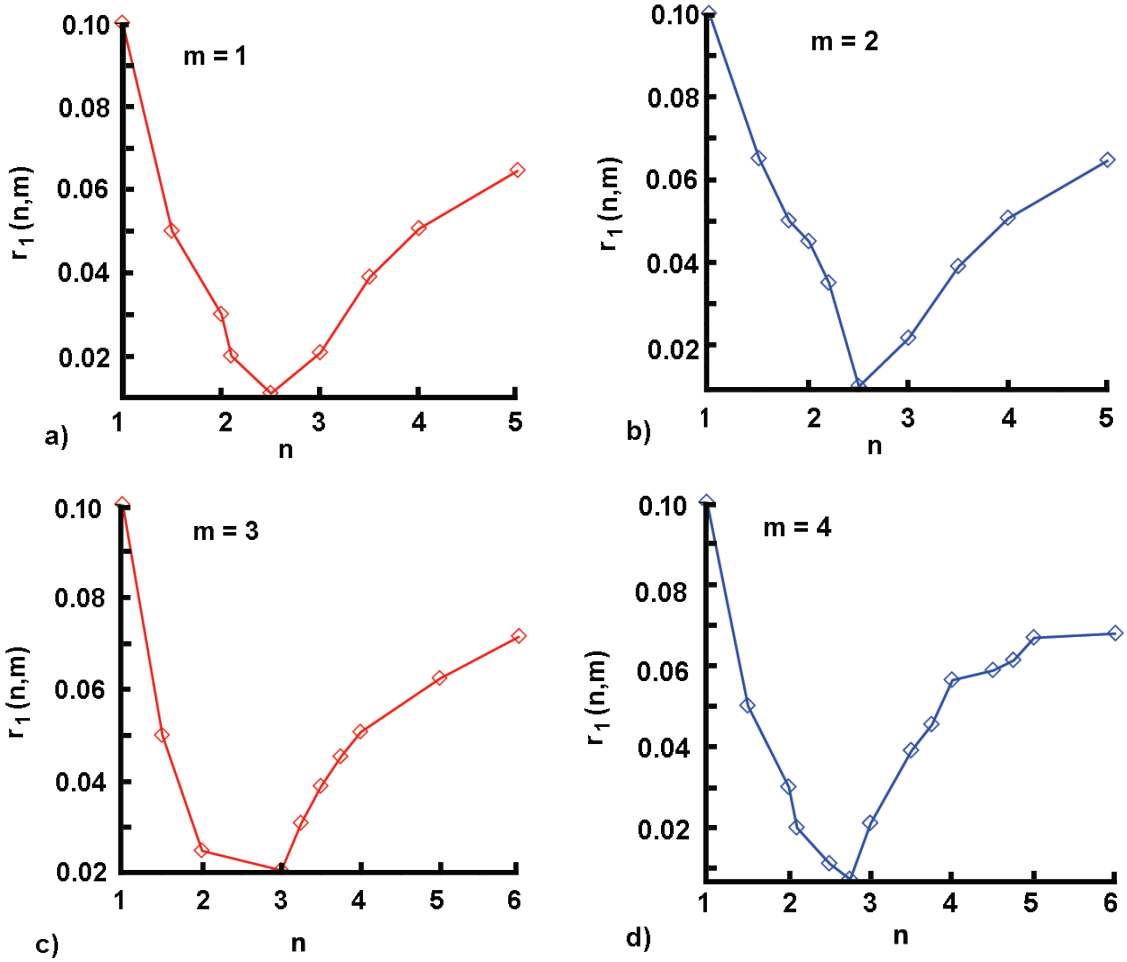

Figure 7. Error measures $r_1(n,m)$ in cases when minimization of e_{L1} is carried out

Optimal n through minimization of L_2

The plots with the optimal exponents presented in Figure 9 as well as the results presented in Figure 10 reveal the same problem as in the case when the optimization is carried out through minimization r_{L1}. Therefore, mainly due to the specific function used as an assumed profile the concept of optimal exponent over the entire range $0 \leq X \leq 1$ does not lead to satisfactory results.

Outcomes of the solution refinement with constant exponent n

It is clear that the refinement procedures looking for an optimal exponent n_{opt} strongly indicate that the results are unacceptable. This can be visually detected, without error presentations, since the approximate solutions are too distant from the reference ones, and therefore a new approach should be found to resolve the situation. As a solution to the emerging problem the next Section 6 develops a concept of a variable exponent dependent on the variable X. This means we need a functional relation $N = f(X)$ where there is an additional parameter allowing easily to adjust the profiles with minimal errors of approximations.

Solution refinement by applying a variable exponent $n = n(X)$

As previously mentioned in the sections preceding this one, our goal is to design functional relationships $n = f(x)$ that are suitable for reaching the goal we have set. We will restrict ourselves to one definition, even though there may be alternatives; this will be sufficient to show

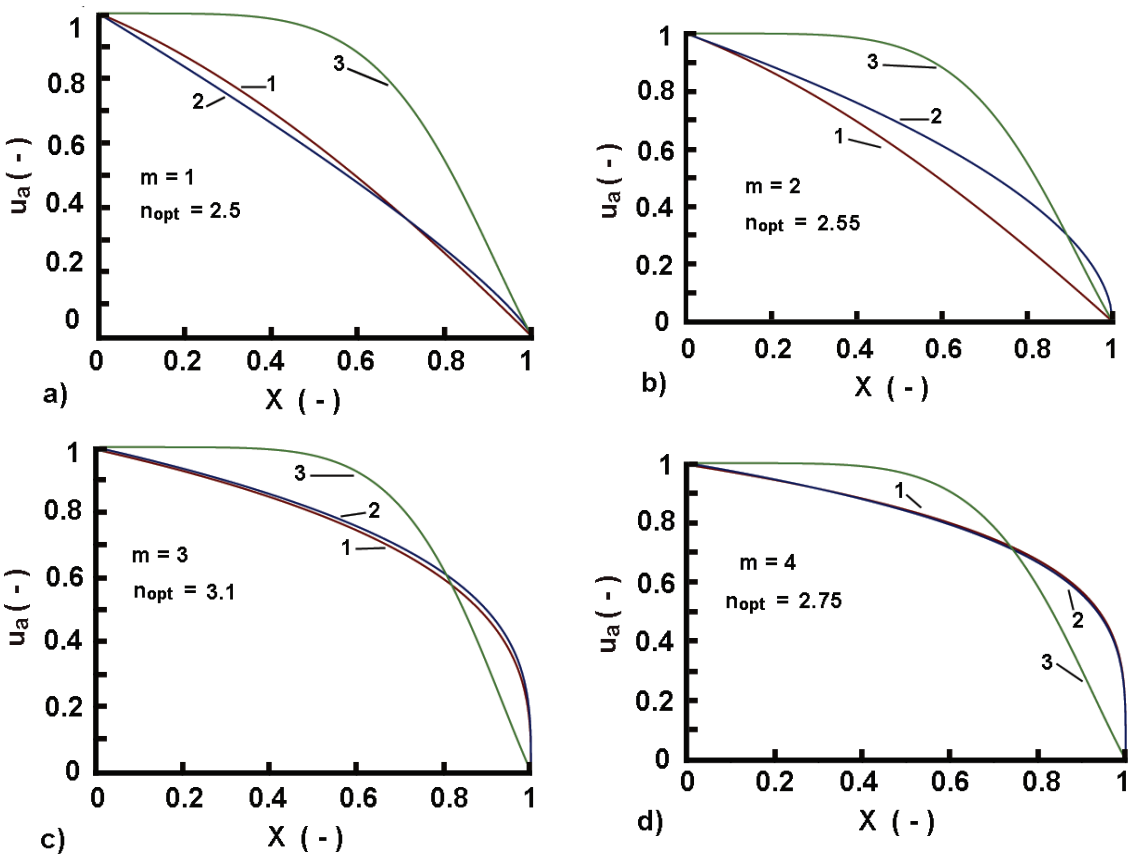

Figure 8. Comparative plots of the approximate solutions (lines 3) with determined optimal values of the exponent n (the values are available in the figure legends), determined through minimization of the E_{RL1} measure, and the solutions developed in [40] (lines 1) and [15] (lines 2). **Note**. For the parabolic profile solutions [15] the optimal values of the profile exponents are: $n(m=1)=0.815$, $n(m=2)=0.537$, $n(m=3)=0.305$, $n(m=4)=0.253$

that the approach envisaged works.

Ad-hoc functional relationship $n = f(X)$ and initial experiments

From the ideas in the above-mentioned suggestions we generate the following $n = f(X)$ functional relationships (conjectures)

$$n_1 = \frac{1}{1-X}, \tag{37}$$

$$n_2 = \frac{1}{1-X^p}, \tag{38}$$

$$n_3 = \frac{1}{1-pX}, \quad p = f\left(\frac{1}{m}\right). \tag{39}$$

All of them are from one family of reciprocal functions: for $q = 0$, n_2 reduces to n_1, while for $p = 1$, n_3 reduces to n_1. Functional relationships $n_3 = f(x)$ are shown in Figure 11 for parameter $p = 1/m$ as illustrative examples. We have to mention that $1/m$ defines the optimal exponent of the parabolic profiles as proved in [15]. As an empirical step towards refining the plots and looking

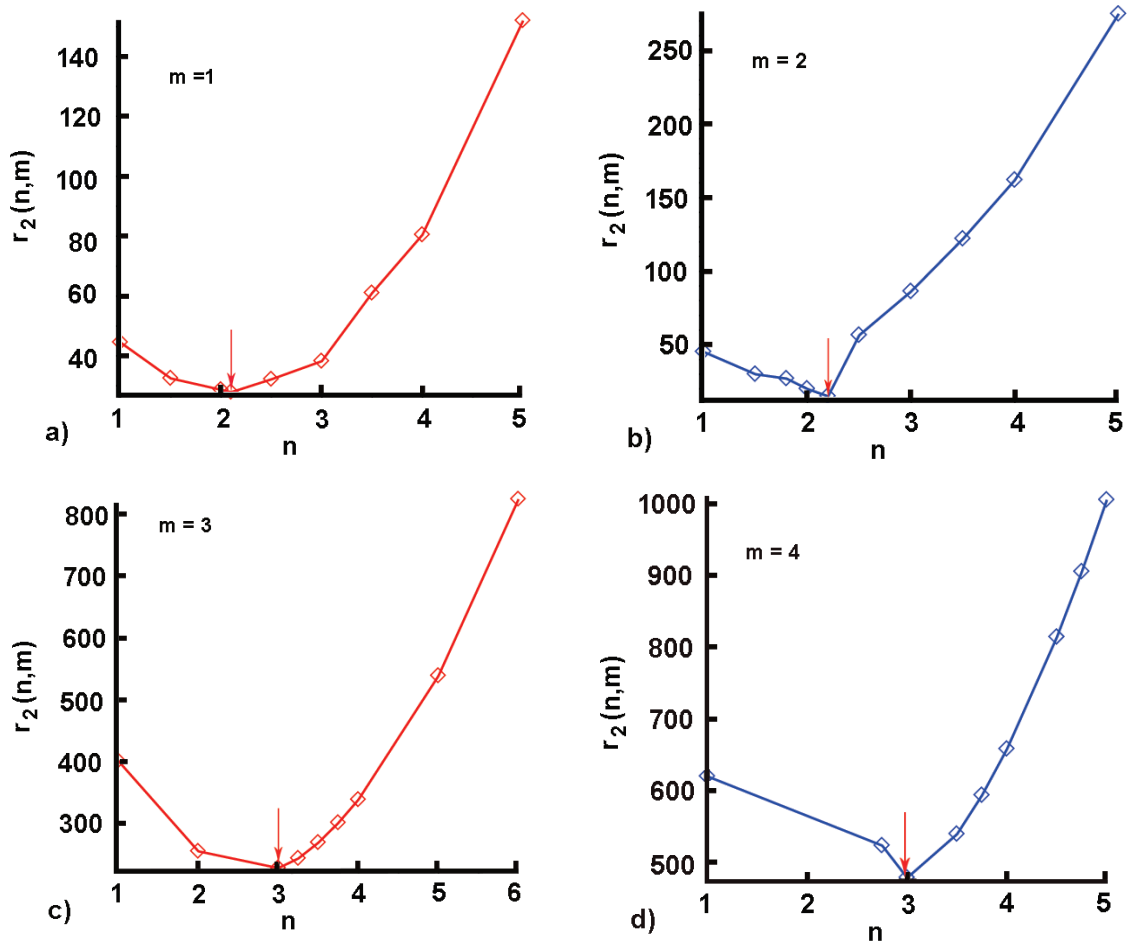

Figure 9. Error measures in cases when minimization of e_{L2} is carried out

for a suitable relationship $p = f\left(\frac{1}{m}\right)$ we can slightly modify the prefactor p in (39) as $p = k_m/m$, where k_m, for now, is an adjustable coefficient. Figure 12 provides a fascinating example of how the shape of the approximation profile defined by (40) may change when the parameter p varies. Now, the plots in Figure 13 show what of this functional relationship would be the promising one leading to the solution improvement. For example, the experiments with n_3, particularly with $m = 4$, revealed an almost good approach to the developed solution to those of Heaslet and Alksne [40] by the moment method, and the parabolic profile approximation [15]. This was attained by the adjustable coefficient $k_m = 3.55$ which means $p = 0.885$. However, the errors of approximation are still not acceptable, even though the shapes of the profiles, precisely when $n_3 = f(X)$ is applied, reveal the desired tendency of how this should be done. Starting from these initial achievements, we go to more precise refinement of the developed approximate solution, as is done in the next section. The solution with n_1 is an extreme case that consists of straight lines, an effect that could be attributed to the fact that for $X \to 1$, we have $n \to \infty$. Intuitively, more suitable for further solution refinements is n_3 allowing to generate smooth profiles (it reduces to n_1 for $p = 1$).

Refined solutions with variable exponents $n = f(X)$

The refinement of the solution developed in this section is based on a semi-empirical approach consisting of two basic elements (steps): The first element is *the developed approximate solution*

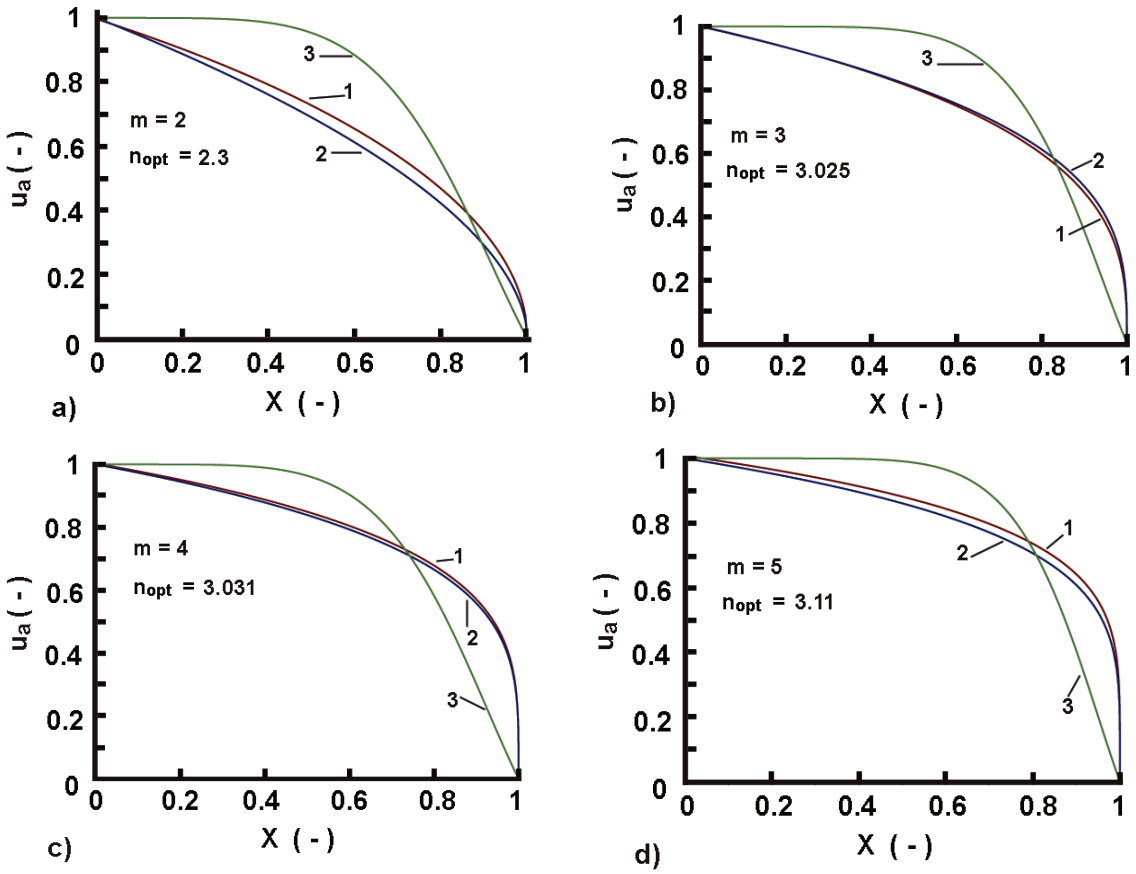

Figure 10. Comparative plots of the approximate solutions (Lines 3) with determined optimal values of the exponent n (the values are available in the figure legends), determined through minimization of the E_{RL2} measure, and the solutions developed in [40] (lines 1) and [15] (lines 2). **Note**. For the parabolic profile solutions [15] the optimal values of the profile exponents are: $n(m = 1) = 0.815$, $n(m = 2) = 0.537$, $n(m = 3) = 0.305$, $n(m = 4) = 0.253$

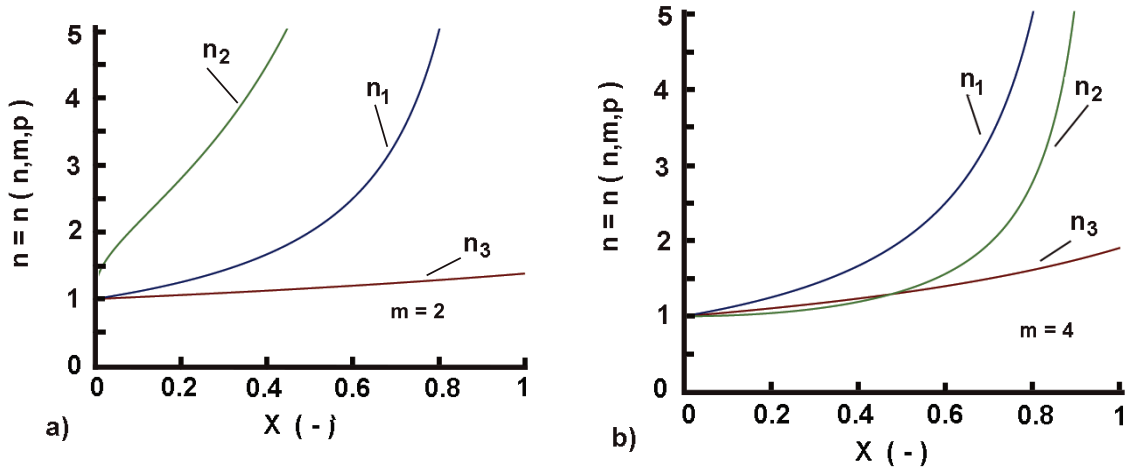

Figure 11. Functional relationships $n_3 = f(X)$, accepting particularly $p = 1/m$. a) For $m = 2$ and b) For $m = 4$

with a constant n. The second step is *to deform this solution with a suitable function* $n = f(X)$. It is worth noting, if some questions and objections would come to mind of the reader, that if at the very beginning of the solution development, the concept of a variable exponent is accepted, the

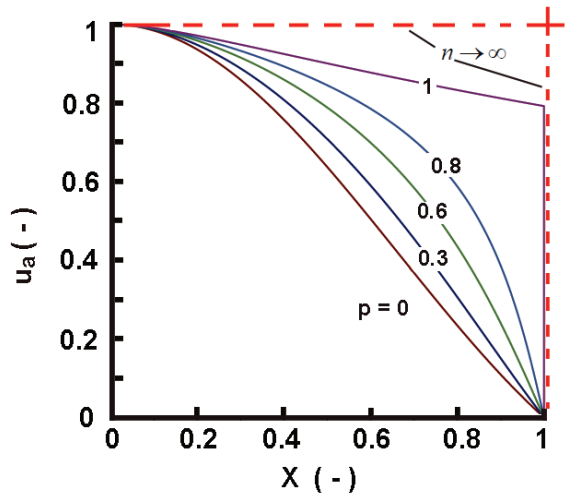

Figure 12. An Illustrative example of how the shape of the approximation profile changes when the parameter p controlling the exponent n through the function (40) varies

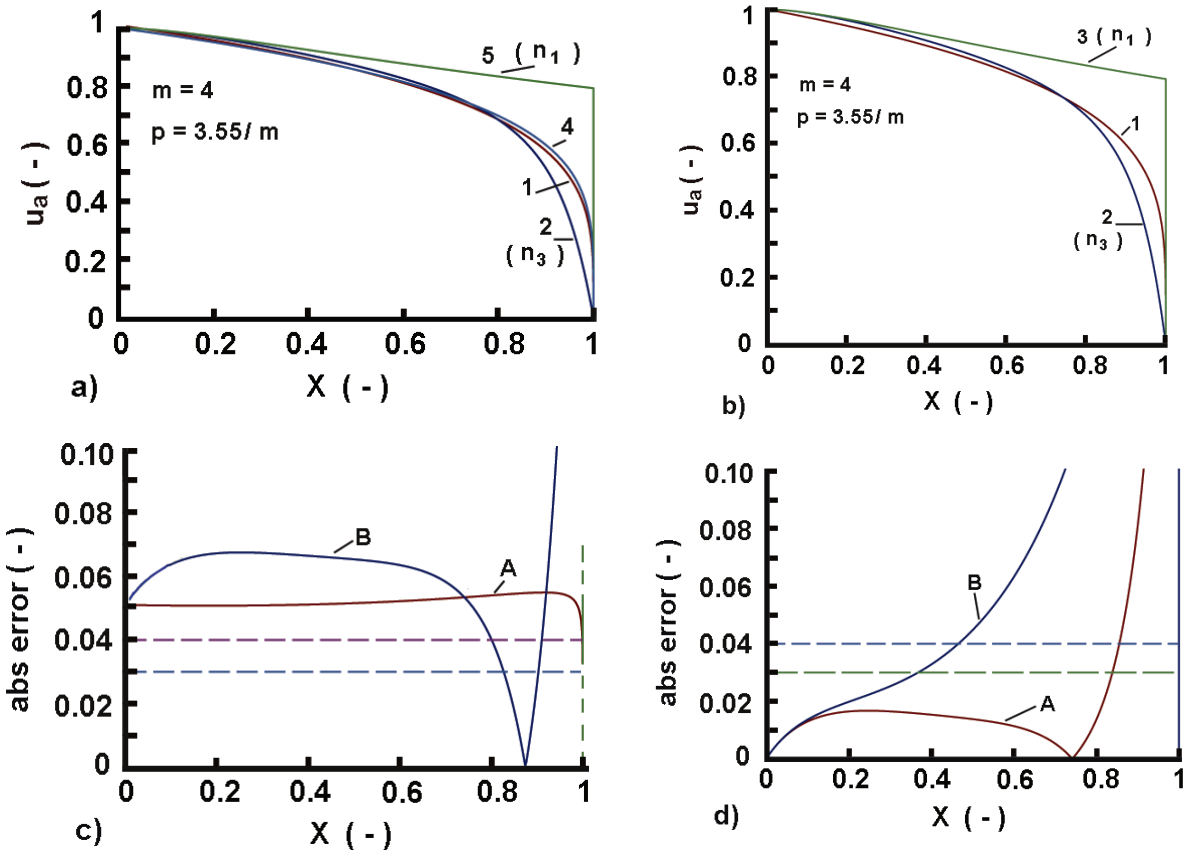

Figure 13. A test: Approximate solutions as functions of the dimensionless variable X demonstrating the effects of the functional relationships $n = f(X)$ on the profile shape and approximation adequacy. First row: a)-A comparison with the Heaslet and Alksne solution [40] (line 1, the red line in the online version). b) A comparison with the parabolic profile solution [15] (line 1, the red line in the online version). Second row: c) Absolute errors of approximation with respect to the Heaslet and Alksne solution [40]: Line A-the solution with n_3, Line B-the solution with n_1; d) Absolute errors of approximation with respect to the parabolic solution [15]: Line A-the solution with n_3, Line B-the solution with n_1. Note: the dashed horizontal lines denote the levels of errors, commonly attainable of integral-balance solutions [15]

integral-balance method would be inapplicable.

Thus, we are directly shaping the assumed profile making *a hybridization of the basic result*, i.e. the approximate solution (32), where all parameters remain unchanged, with the exponent n as a function of the variable X. That is, we have a modified version of the approximate solution

$$u_a = \frac{\sin(\pi X^{n(X)})}{\pi X^{n(X)}}, \quad n = \frac{1}{1-pX}, \quad 0 \leq X \leq 1, \quad 0 < p < 1. \tag{40}$$

The optimization procedure was carried out by minimization of the residual function, concerning optimal values of the parameter p, based on the new assumed profile, through numerical simulations. The form of the residual function is skipped here due to its cumbersome expression but for the sake of clarity derivatives of (40) are available in Appendix 9.

The plots in Figure 14, with optimal values of the parameter p (see the figure legends), reveal quite acceptable errors when compared to the reference solutions (we have to remember that they are also approximate) from [40] and [15]). The plots of the approximation errors are shown in Figure 15.

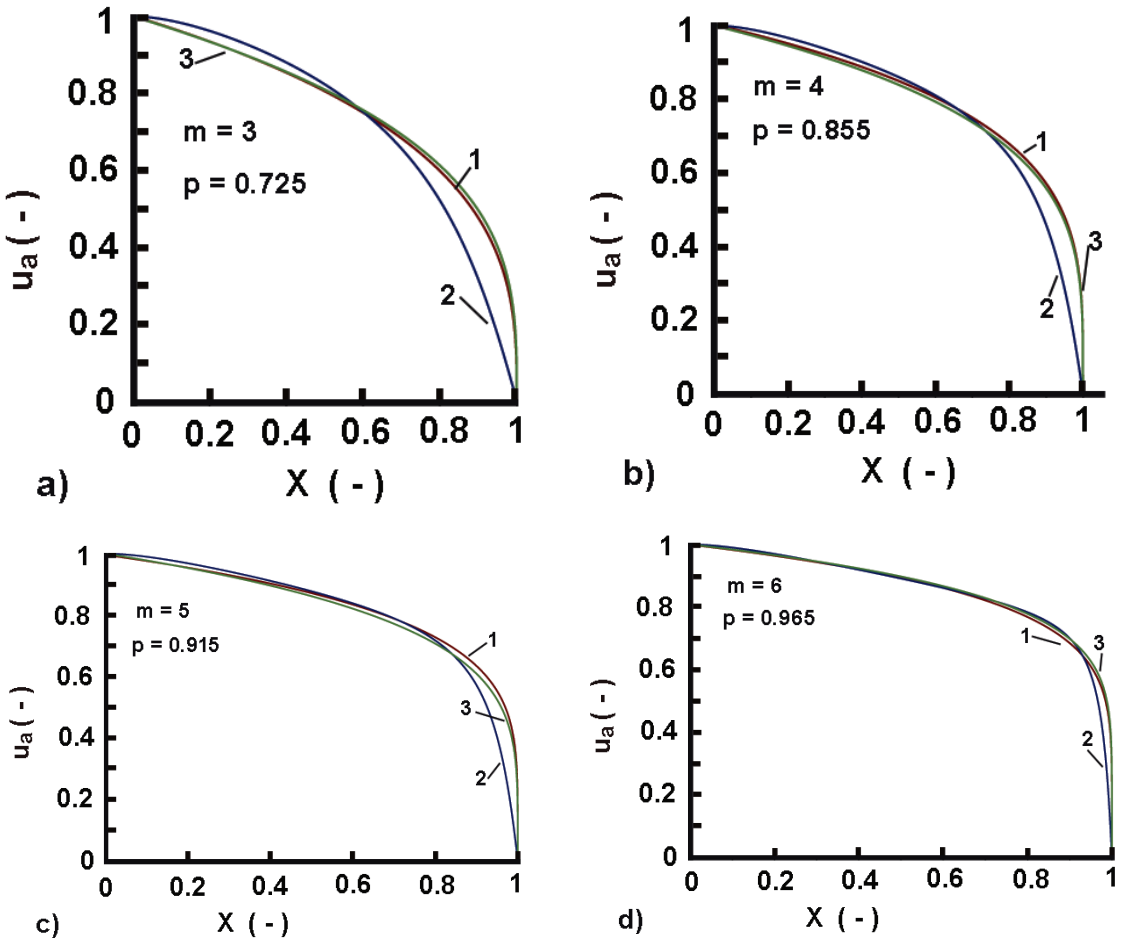

Figure 14. Approximate solutions (lines 2, in green colors) as functions of the dimensionless variable X with optimal values of the parameter p (see the figure legends) compared to the reference solutions of Heaslet and Alksne [40] (lines 1, in red colors) and parabolic profile solutions (DIM) from [15] (lines 2, in blue colors)

It is evident that the idea of a variable exponent $n = f(X)$ functions well. Considering that it had been used just once before (to the situation of $m = 0$) [41], in a slightly different manner, this is

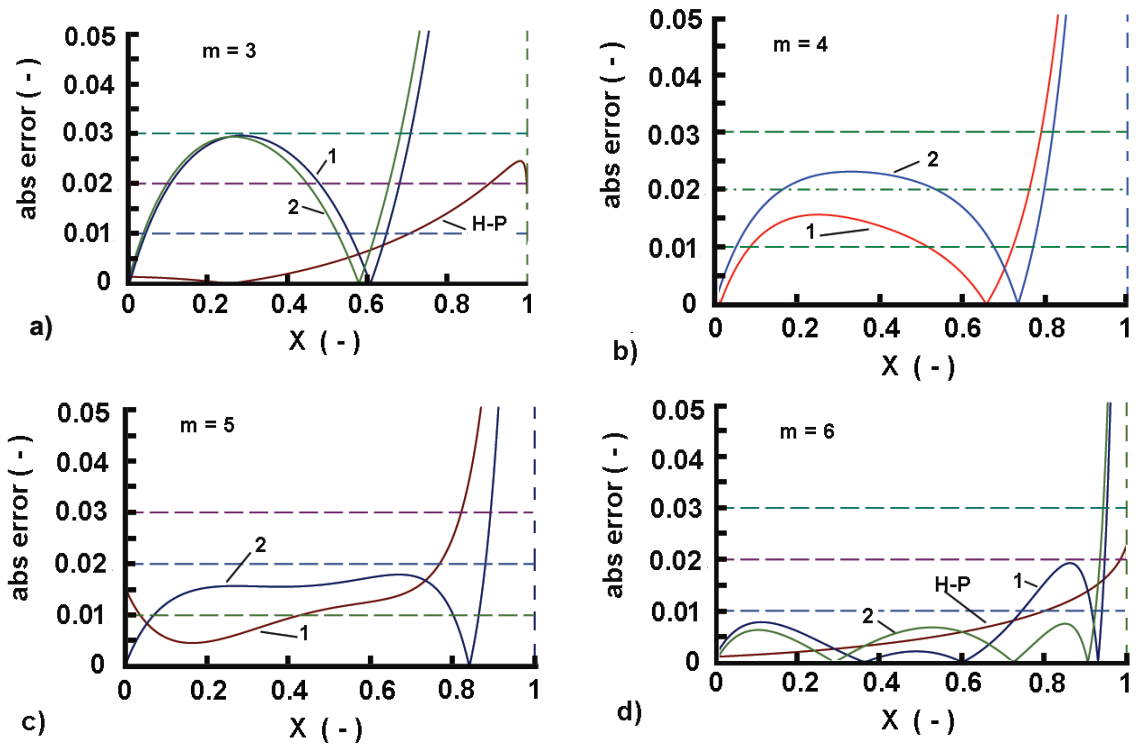

Figure 15. Errors of approximations as functions of the dimensionless variable X with optimal values of the parameter p (see the figure legends in Figure 14) concerning the reference solutions of [40] (lines 1) and [15] (lines 2). **Note:** Line H-P in panels a) and d) indicates the error of the parabolic profile solution [15] concerning that in [40]. The vertical dashed lines at $X = 1$ mark the asymptotes of the errors

a good outcome. Notably, the approximation errors increase significantly in proximity to point $X = 1$, where the steep fronts result in extremely high solution gradients $\partial u_a/\partial X$. All approximate solutions of (1) share this characteristic, though (see [15] and the examples therein).

A test for high value of m

As we increase the amount of m, we come to a scenario where the $Sinc_\pi(\pi x^{n(x)})$ profiles and the plots of the solutions of Heaslet and Alksne [40] are almost identical (visually) close to the form (see panels a) and c) in Figure 16), am small differences at the middle range of the interval $0 < X < 1$. Further, we can see a similar result when plotting $Sinc_\pi(\pi x^{n(x)})$ approximation (panel c)) in Figure 16) and the solution utilizing a parabolic assumed profile (with $n_{opt} = 1/m = 0.1$, as per [15]), with errors acceptable only for small values of X. Based on the final results, we can conclude that the assumed profile $Sinc_\pi(\pi x^{n(x)})$ produces approximations comparable to the parabolic profile-based solution. However, it is worth noting that when the two reference solutions are plotted (Figure 17-panel a)) the lines are indistinguishable, but the magnification of two sectors (Figure 17-panels b) and c) clarify the situation. It is worth noting that the absolute difference between them is well distributed along the abscissa, with an increase close to the front, but this is inherent for all approximate solutions concerning the model (1).

Some insights concerning the optimal values of the optimal parameter p

The results developed to this point satisfy our main task, and we may raise the following reasonable question: Is there a functional relationship between the optimal values of the parameter p and the non-linearity exponent m? The plot in Figure 18 shows a saturation of the values of p, approaching unity as m is increased (panel a). However, we recall that (as mentioned earlier) when the parabolic profile is used [15] the optimal exponents of it obey the so-called $1/m$ law (section 5.3 and Figure

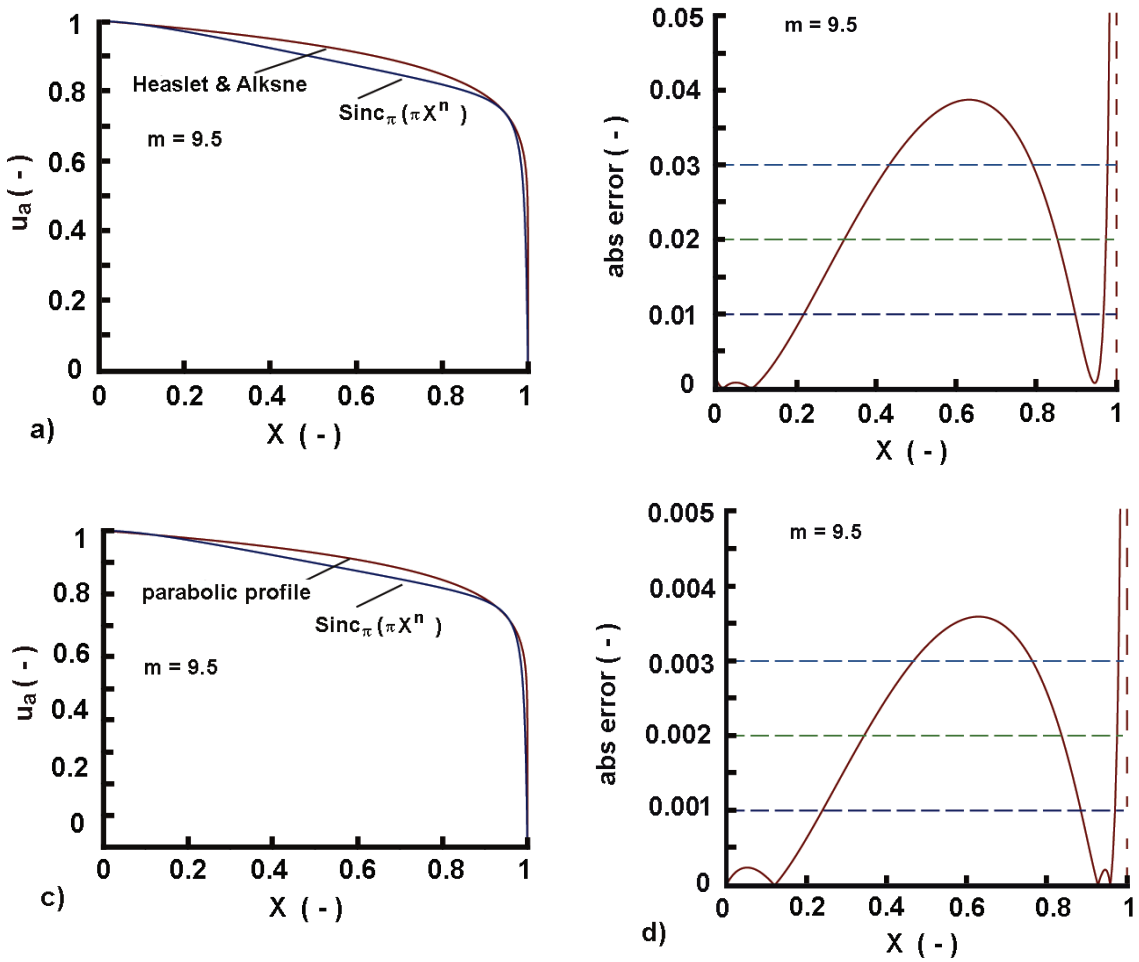

Figure 16. Approximations at high values of the exponent m. Comparisons between the present approximations and the solution of [40] and the parabolic assumed profile solution [15] : a) and b) Plots of Heaslet-Alksne solution and $Sinc_\pi(\pi x^{n(x)})$, and errors; c) and d) Plots of the solution based on parabolic profile and $Sinc_\pi(\pi x^{n(x)})$, and errors; **Note:** for the parabolic profile solution $n_{opt} = 1/m = 0.105$; For the $Sinc_\pi(\pi x^{n(x)})$, $p_{opt} = 0.991$

15 in [15]) exhibiting an almost hyperbolic relationship $n_p\,(opt) = f(m)$. Now, taking into account that $0 < p < 1$ and $0 < 1/m < 1$ we see a similar, almost hyperbolic, relationship when the relation $p = f(1/m)$ is plotted (panel b). However, an attempt to correlate statistically the obtained data about the optimal values of p yields a good fit with the Pareto function (panel c) (with the help of SigmaPlot statistics), namely

$$p = 1 - \left(\frac{1}{m^a}\right), \tag{41}$$

where $a = 1.358$, with $P < 0.0001$ and $R = 0.987$, and a standard error of estimate 0.11.

This is a very rough result based on a limited number of numerical experiments, but it allows us to see the versatility of the suggested functional relationship $n = f(X)$, precisely $n_s = f(X)$ and we will comment on it in some detail. It is well known [15], and the plots in the preceding sections show that, when m is increasing, the profile front becomes more and more steep, and its shape is approaching at high m an almost rectangular form. The correlation (41) for high values of m reveals that $p_{m\to\infty} \Rightarrow p \to 1$ (or, in other words, $p_{(1/m)\to 0} \Rightarrow p \to 1$), and therefore $n_{m\to\infty} \Rightarrow \frac{1}{1-pX} \to \frac{1}{1-X}$. That is, with the increase in m, the parameter p approaches values close, but less than 1. The case $p = 1$ is extreme, as demonstrated by the simulations done before (see

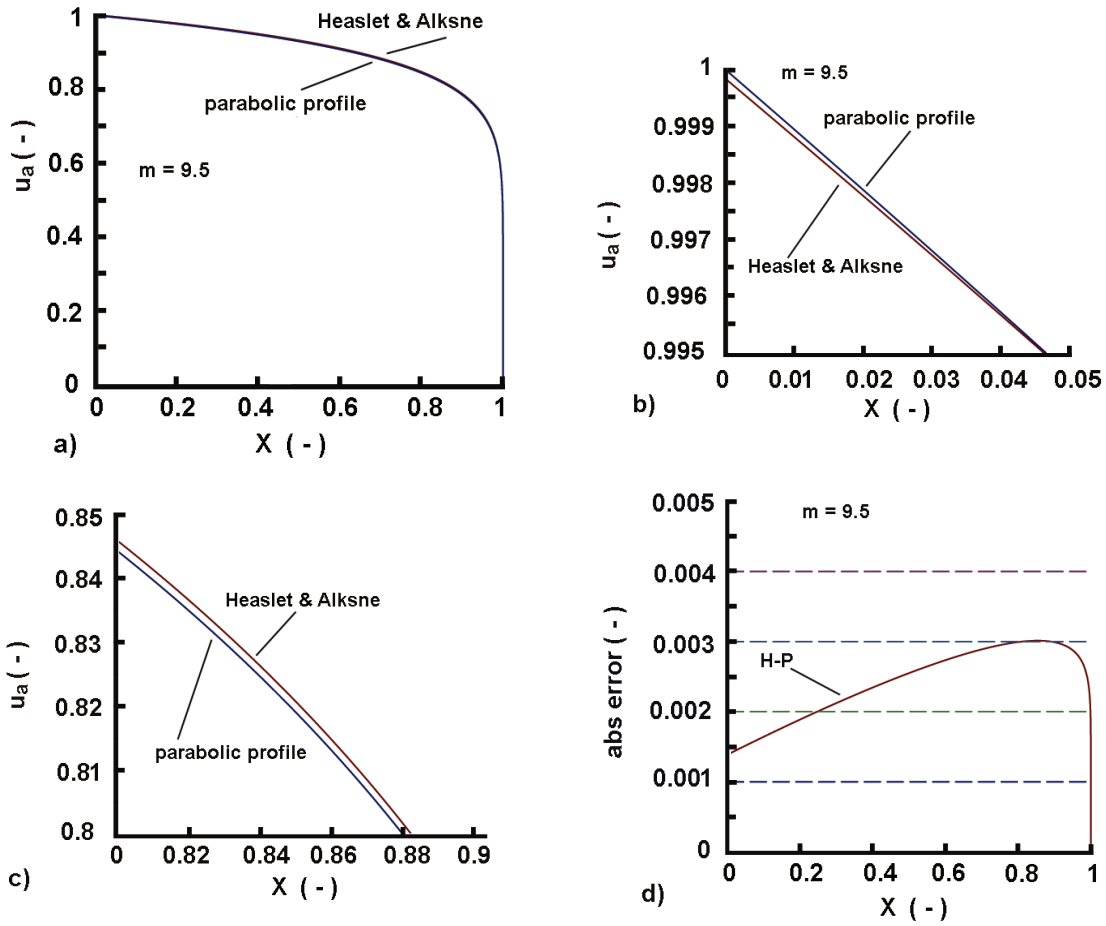

Figure 17. A comparison of the two reference solutions at high values of the exponent m. a) Practically indistinguishable plots; b) A magnification of a sector for small X; c) A magnification of a sector for X approaching 1; d) The absolute error between the two reference solutions. **Note:** 1) for the parabolic profile solution $n_{opt} = 1/m = 0.105$. 2) It is important to know that the solution of Heaslet and Alksne does not match 1 when $X = 0$; this an inherent feature of this solution when computing

Figure 12 and Figure 13, for instance).

7 Comparisons with other available solutions

Now, it is almost mandatory to see how the developed approximate solutions differ or match existing ones published in the literature for some particular values of the parameter m.

The common approach in the solutions used in the benchmarking

On the character of the benchmarking solutions

To verify the validity of the developed approximate solutions we are obliged to compare them to those available in the literature. No closed-form solution to the model (1) exists [42, 43] and the first solution provided by Philip [44] is hybrid by an analytical step and numerical solutions (see details in [42]).

In the case of the fixed temperature boundary condition (Dirichlet's problem) most of the available solutions allowing benchmarking [40, 42–49], as first step, utilize the Boltzmann transformation $\eta = x/t_*^{1/2}$, where $t_* = D_0 t$, to transform (1) into a non-linear ODE, solved them analytical or numerically. This allows us easily to compare the integral balance solution to them since it intrinsically generates expressions in terms of η (see Eq. (32)).

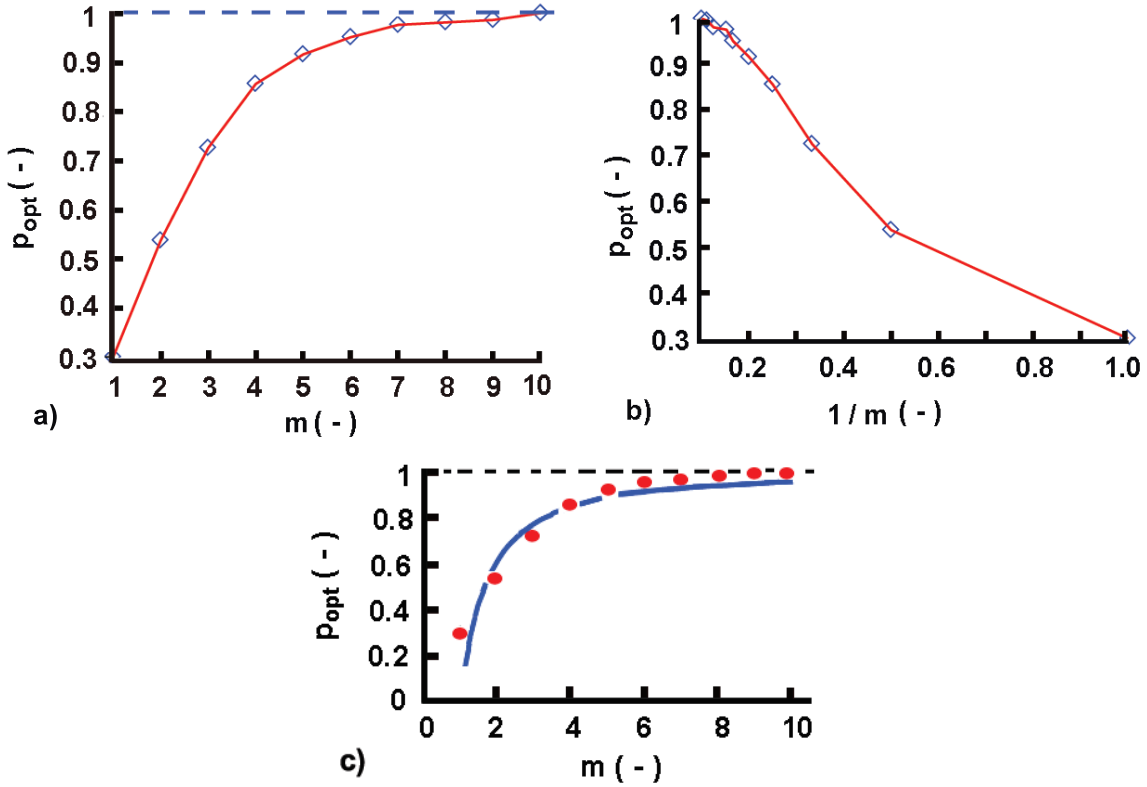

Figure 18. Relationships of the optimal values of the parameter p and the parameter m. a) $p_{opt} = f(m)$; b) $p_{opt} = f(1/m)$; c) $p_{opt} = f(1/m)$ correlated by (41). **Note:** In a) and b) the points are linked by straight lines, as this is provided by Maple, while in c) the data fit that was done is what made the fitting smooth

The present solution in terms of η and calculation issues

In the context of benchmarking the new solution is represented in terms of the similarity variable η and the variable exponent $n = f(p, X) = 1/(1 - pX)$ as

$$u_a = \sin\left(\frac{\pi\left(\frac{\eta}{\sqrt{S_2(m+1)}}\right)^{n(\eta)}}{\pi\left(\frac{\eta}{\sqrt{S_2(m+1)}}\right)^{n(\eta)}}\right), \quad n(\eta) = \frac{1}{1 - p\left(\frac{\eta}{\sqrt{S_2(m+1)}}\right)}. \tag{42}$$

Applying (42) we have to stress the attention to an implicit problem concerning calculations of S_2 because the variable exponent $n = 1/(1 - pX)$ is controlled now by the parameter p. Starting from $X = 0$ we have $n(X = 0) = 1$ and then towards $X = 1$, we have rising values of n up to $n(X = 1) = 1/(1 - p)$. Thus, the value of S_2 should be calculated for $n = 1$ (see Section 4), thus giving its initial value, and the determined optimal value of the parameter p should be used.

Comparison to the series solution of Brutsaert and Weisman

Brutsaert and Weisman [48], applying the Boltzmann similarity variable $\eta = x/\sqrt{a_0 t}$ transformed the model (1) to

$$\frac{d^2}{d\eta^2}\left[\frac{B^{m+1}}{m+1}\right] + \frac{\eta}{2}\frac{dB}{d\eta} = 0. \tag{43}$$

With this transformation, the new boundary conditions are: $B = 0$ for $\eta \to \infty$ and $B = 1$ for $\eta = 0$. Brutsaert and Weisman [46, 47] were concerned with the accuracy of both Philip's numerical solution [44] and the solution of Heaslet and Alksne [40]. As an outcome of this analysis, they did an approximation for $\eta \to 0$ [46], which is close to the boundary$x = 0$ where $B = 1$, namely

$$B_1 = \left\{ 1 - \eta \left[\frac{(m+1)^2}{2\,(m+2)} \right]^{\frac{1}{2}} \right\}^{\frac{1}{m+1}}. \tag{44}$$

Further, a second approximation close to the front of the penetration layer $\eta \to \eta_B = \delta$, $B \to 0$, yields (here we use the symbol δ instead η_F as in the original work, for consistency with the entire analysis of the new solution developed)

$$\frac{d^2}{d\eta^2}\left[\frac{B^{m+1}}{m+1}\right] + \frac{\delta}{2}\frac{dB}{d\eta} = 0, \quad B = B^m \frac{dB}{d\eta} = 0, \quad \eta > \eta_B, \tag{45}$$

with a boundary condition beyond the front (η_B in the original work corresponding to $\sqrt{S_2\,(m+1)}$ in the new solution),

$$B = B^m \frac{dB}{d\eta} = 0, \tag{46}$$

which is equivalent to the Goodman condition $\partial\theta\,(\delta)/\partial x \; = 0$.

In this case, the front is defined by $\delta = \eta_B = (2/m\,)^{1/2}$ resulting in the following approximation

$$B_0 = \left(1 - \eta\sqrt{\frac{m}{2}}\right)^{\frac{1}{m}}. \tag{47}$$

It is worth noting, that the approximation is the first term of the series solution of Heaslet and Alksne [40].

The plots in Figure 19 present DIM solutions with two assumed profiles (with a parabolic profile (9) developed in [15] and the present $\mathrm{Sinc}_\pi\,(\pi X^n)$, with $n\,(\eta)$) and the B_1 approximation. The plots reveal strong differences for high values of η, and only for $m = 3$ the plots are close to each other. However, we have to remember that the B_1 approximation is for $\eta \to 0$, and practically works for small η, practically for $\eta \leq 0.4$. The discrepancies appear when $\eta \to 1$ and further, that is beyond the range where B_1 was developed, for other values of m, and this could be attributed to the solution methods applied: the initial transform with the Boltzmann similarity variable, for instance, yields a non-linear differential equation needing some approximation to find expressions such as $B1$. On the other hand, the DIM solutions, with either a parabolic profile or that based on the modified *sinc* function, intrinsically generate this similarity variable.

The tests in Figure 19 seem discouraging, but a deep analysis of the structure of the compared solutions and the techniques for their development allows us to find the right way how they should be compared.

$$B_1 = \{1 - X_{B1}\}^{\frac{1}{m+1}}, \quad X_{B1} = \frac{\eta}{\sqrt{\frac{(m+1)^2}{2(m+2)}}} = \frac{x}{\sqrt{a_0 t}\sqrt{\frac{(m+1)^2}{2(m+2)}}}, \quad 0 \leq X_{B1} \leq 1. \tag{48}$$

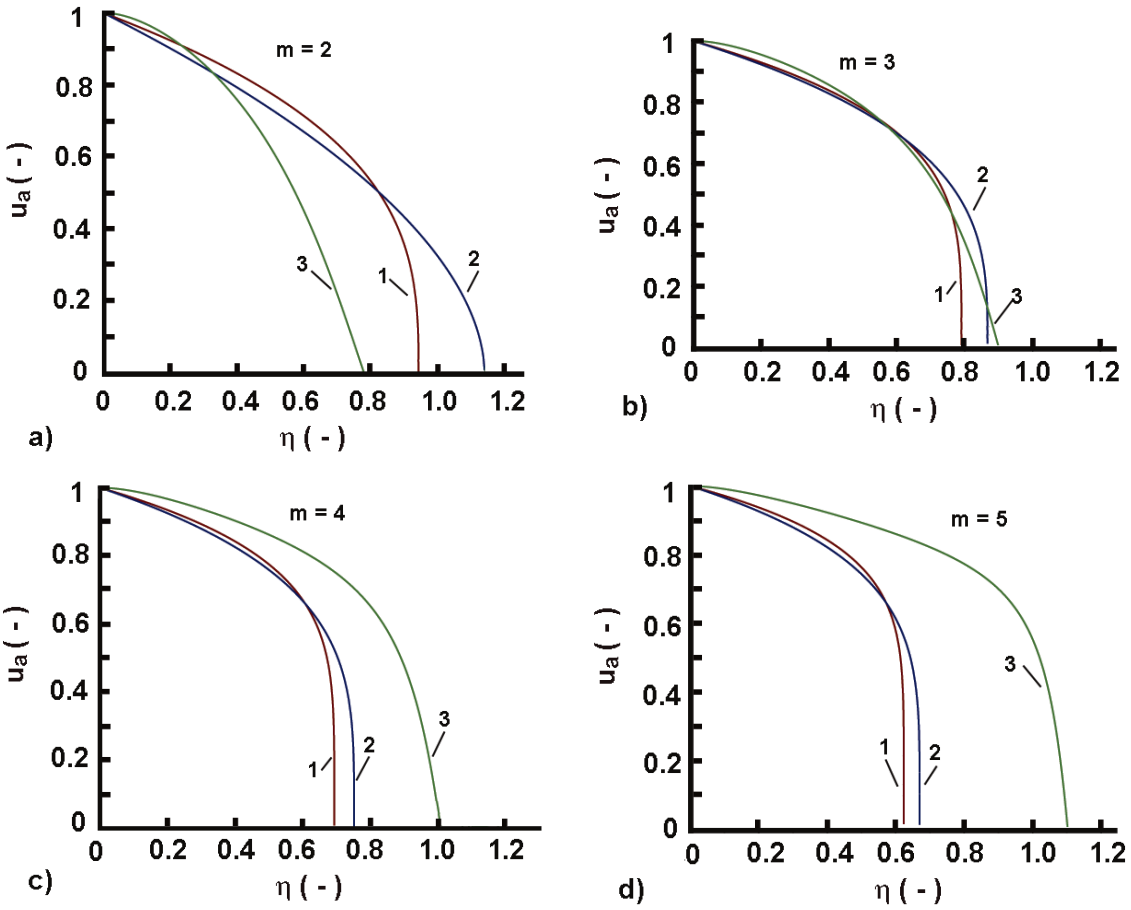

Figure 19. Comparative presentations of the newly developed solution (lines 3, green in online version), the approximation B_1 of [46] (lines 1, red in online version) and DIM solutions based on parabolic profile (lines 2, blue in online version), as function of the similarity variable η. **Note:** For the solutions based on a parabolic profile, we have values of n_{opt} available in the preceding sections

In the light of the basic idea of this study, the approximation B_1 can be presented as

$$U_{parabolic} = \left(1 - X_{parabolic}\right)^{n_{opt}}, \quad 0 \leq X_{Parabolic} \leq 1, \tag{49}$$

$$X_{parabolic} = \frac{\eta}{\sqrt{\frac{(n_{opt}+1)(n_{opt}+2)}{m+1}}} = \frac{x}{\sqrt{a_0 t}\sqrt{\frac{(n_{opt}+1)(n_{opt}+2)}{m+1}}}. \tag{50}$$

With this common manner in the presentation of solutions developed by different techniques, we get the plots in Figure 20. The results are rather encouraging, and we can see, as we saw the same behavior earlier, that with the increase in the value of m all solutions are very close to each other. We do not show the errors between them since, for instance, this was already done by comparing the present solution and that based on the parabolic profile.

Immediately, the following key question comes to mind: Are X_{B_1}, $X_{Parabolic}$, and X_{Sinc}, as defined above, equal? All solution techniques commented on here use the concept of a final penetration depth (we use the common symbol δ). The solutions are then shown by all of them as functions of the ratio x/δ. *We have the same physically defined penetration depth* in every case, *irrespective of how*

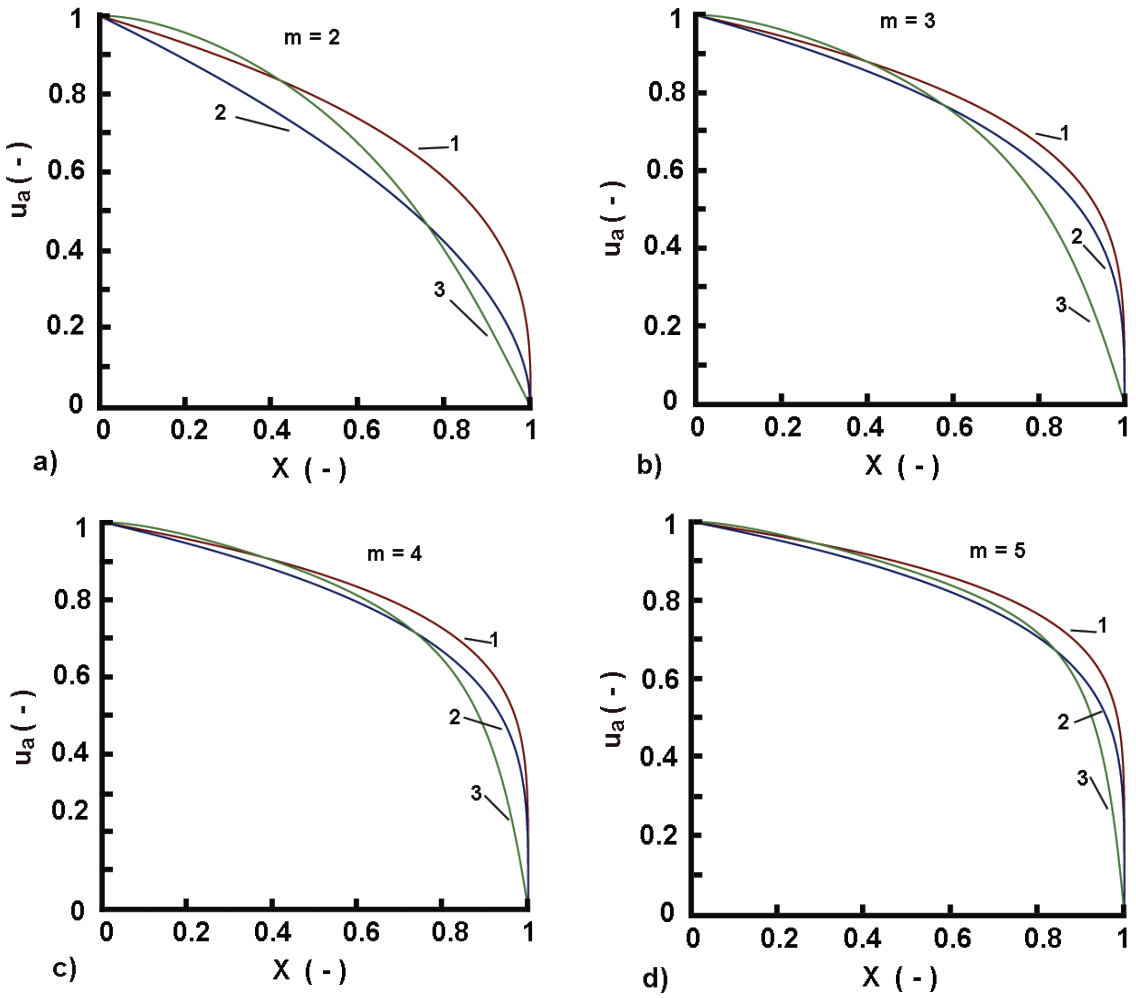

Figure 20. A unified approach to compare the newly developed solution (lines 3, green in online version) with the approximation B_1 of [46] (lines 1, red in online version) and DIM solutions a based on parabolic profile (lines 2, blue in online version)

the penetration depth is expressed as a function of the model's parameters and the value of m. Therefore, $X_{B_1} = X_{Parabolic} = X_{Sinc}$ is the answer that closes the point.

Turning again on the problem emerging with plots in Figure 19, when we extract the similarity variable η from the ratio $x/\delta = X$, as a prefactor, we get different denominators strongly depending on the solution approach. They have no physical meaning, and therefore we cannot expect them to be equal; This is clearly seen from the points where the lines cross the abscissa in Figure 19. However, in contrast, the diffusion layer depth δ should be the same, in all cases and solutions, because it is a physically defined distance of diffusant penetration.

As a result, we can close this section by noting that the newly generated solution is equivalent to the ones that already exist. The only way for us to arrive at this conclusion is to identify what they have in common and how their structures can be expressed coherently, as we did briefly above.

Comparison to Tuck's approximate solution

For the special case with $m = 2$, concerning diffusion of Zn and $GaAs$ in silicon Tuck [49] has developed two approximations of the diffusion profile, marked as T_1 (51) and T_2 (52) , accordingly

$$T_1: \quad \eta = \frac{x}{\sqrt{D_0 T}} = \frac{\left(e^2 - e^{2u}\right)}{\sqrt{30.99}} \Rightarrow u = \frac{1}{2}\ln\left(e^2 - \eta\sqrt{30.99}\right), \quad 0.4 < u < 1, \tag{51}$$

$$T_2: \quad \eta = \frac{x}{\sqrt{D_0 T}} = 1 - u^2 \Rightarrow u = \sqrt{1-u}, \quad 0 < u < 0.4. \tag{52}$$

The plots in Figure 21-panel a), present T_1 and T_2 parallel to the DIM solutions with a parabolic profile [15] and the new solution. The absolute errors (Figure 21-panel b)) between T_1 and the DIM solutions is less than 0.03 in the range $0.4 < u < 1$ (the horizontal dashed line in Figure 21-panel b)), corresponding to $0 < \eta < 0.4$ (the vertical dashed line). With T_2 the absolute point-wise difference may reach about 0.05 in the range $0 < \eta < 0.4$ (the vertical dashed line). The point-wise differences sharply increase beyond these ranges. Unfortunately, Tuck's approximations

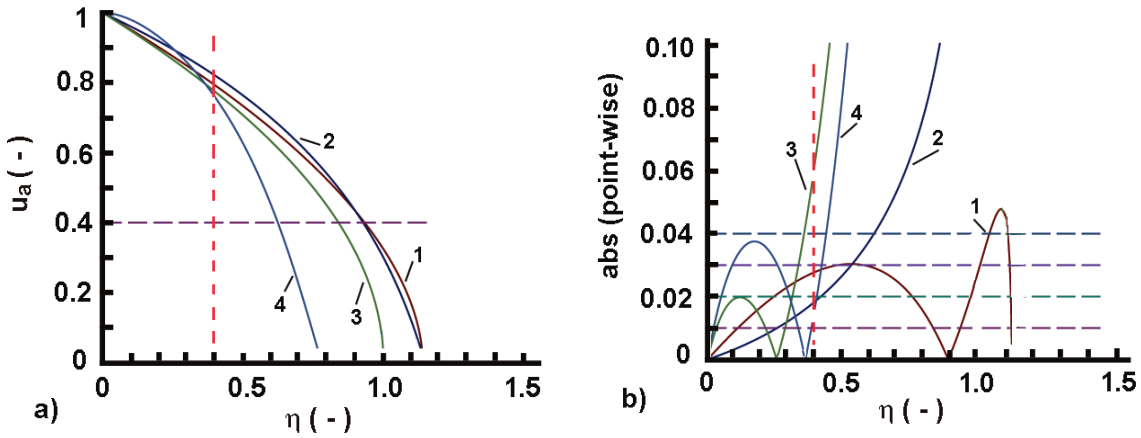

Figure 21. Comparative plots in terms of similarity variable η: a) The new solution (line 4), Thuck's approximations T_1 (line 2), T_2 (line 3) and the DIM solution with a parabolic profile (line 1). b) Point-wise errors between the approximations. line 1: T_1-DIM (parabolic profile), line 2: T_2-DIM (parabolic profile), line 3: T_1-New solution, line 4: T_2-New solution. **Note:** The horizontal dashed lines in panel b) mark the levels of the point-wise differences

cannot be transformed into a unified form, as it was done with Brutsaert-Weisman solutions in the preceding section, due to a missing complete expression of the developed solution. However, the comparative plots reveal the adequacy of the new solution within the ranges of variation of η marked by Tuck.

Benchmarking against the results of Weisberg and Blanc (Philip's solution)

Weisberg and Blanc [45] completed a study on zinc diffusion into GaAs and employed Philip's numerical method [44] to solve the model (1). The new solution in Figure 22 compares the numerical data extracted from Table 1 in [45] (there are also numerical data in [48], produced by the same method, but not presented here). It is worth noting to stress the attention that all numerical solutions commented on in this section are in tabular forms using $\eta/2 = x/\sqrt{(4a_0 t)}$ as an independent variable (this is an effect of the work of Crank [42]) instead of $\eta = x/\sqrt{(a_0 t)}$ used here, and this needs careful rescaling the plots when comparing data.
The plots in Figure 22 reveal that as m increases, the solutions employing an assumed profile got closer to the numerically obtained results. Remember that the initial idea of this study envisaged models where large values of m yield almost rectangular concentration profiles.

Benchmarking against the results of Parlange et al. [50]

To complete this section, we must give due credit to Parlange et al. [50], who examined numerical solutions with m up to 10 massive tabular data for scenarios where the diffusivity functional relationships differed. In Figure 23 and Figure 24, the present solution for applying the $Sinc_\pi\left(\pi X^n\right)$

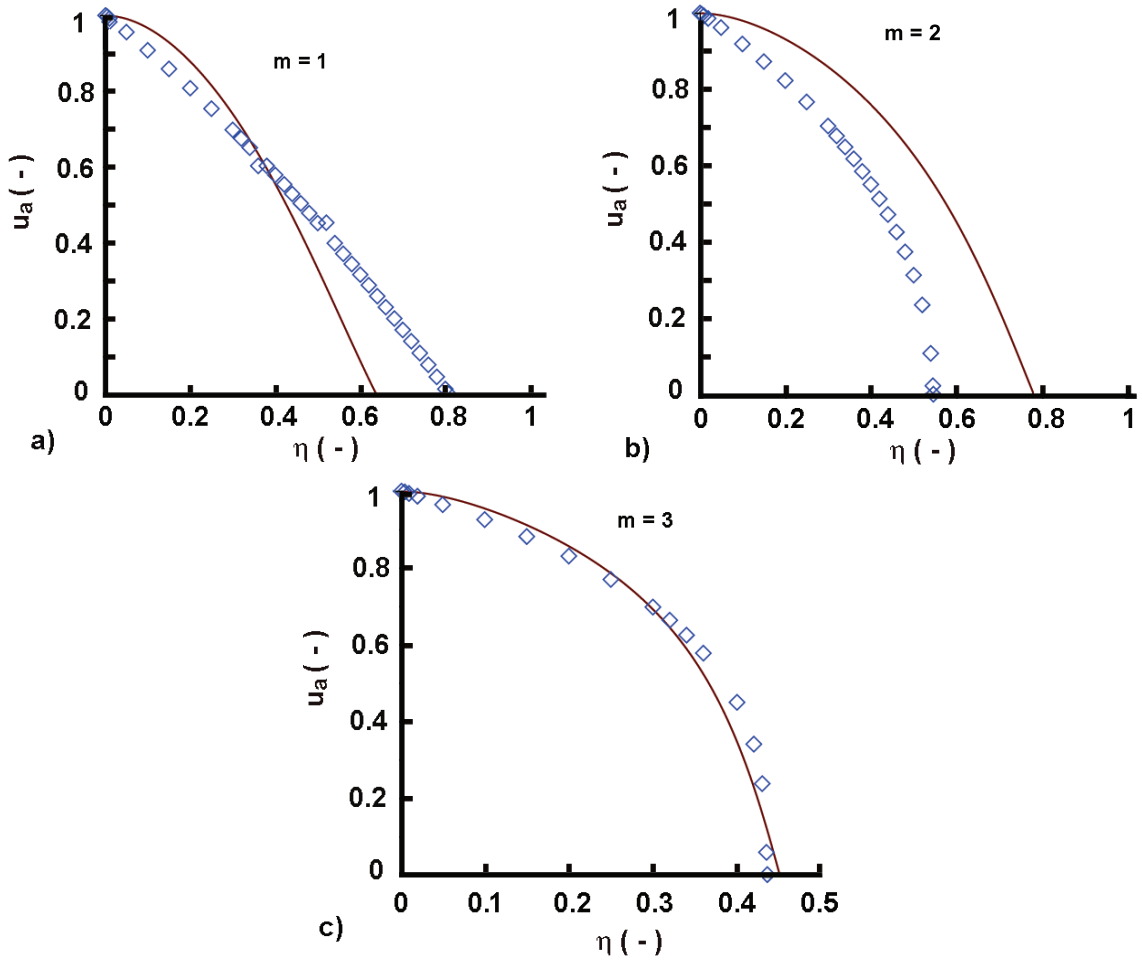

Figure 22. Comparison of the new solution (solid lines) to the numerical results (points) of Weisberg and Blanc [45] a) case for $m = 1$; b) case for $m = 2$; c) case for $m = 3$. Note: Because the points of the numerical solutions for different values of m are too close to in certain places, we present separate plots for each case

as an assumed profile is compared with the numerical data from Table 2 of Parlange et al. [50]. As mentioned, the plots show that the new solutions get closer to the numerical ones as m increases in value (see Figure 24). That is, the new assumed profile will be applied more successfully to the greater m. It is important to mention that in Figure 23 and Figure 24 a rescaling of the present solution using $\eta\sqrt{t}(m = 1)$ was done because a deep analysis of the methodology in [50] reveals that such an effective similarity variable was used as a product of the solutions (both numerical and analytical) performed. To some extent, the results of this comparative analysis could be disappointing, especially the ones when $1 < m < 6$. However, we have to stress the attention on the fact that the solutions developed in [50] use too many approximations and a not well-defined numerical method, thus too many sub-problems may affect the final results. The fact that the new solution is consistent with the two key reference solutions of Heaslet and Alksne [40] and that which is based on the parabolic assumed profile [15], remains essential, albeit this.

8 Concluding remarks, a summary of results and some lines of future research

After this long study with an innovative implementation of a modified $\sin c(x)$ as an assumed profile in an approximate integral-balance solution to a non-linear diffusion equation, we have to strike the balance and outline the new moments and the main results.

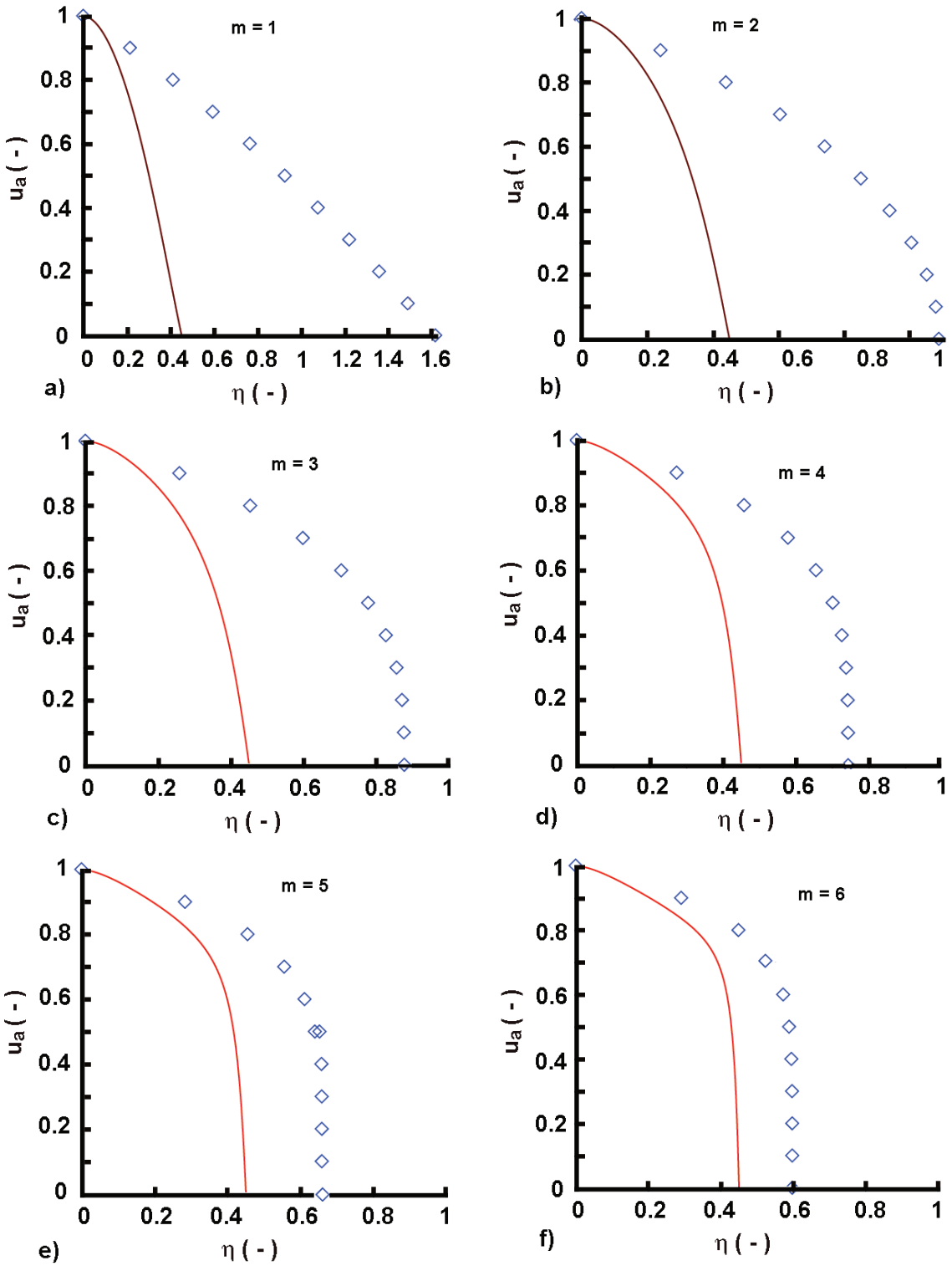

Figure 23. Comparison of the new solution (solid lines) to the numerical results (points) of Parlange et al. [50] for low and moderate values of m up to $m = 6$

New moments in the solution approach

The new moments in the approximate solution developed can be outlined as:

- The integral-balance method and its double integration technique are well-known, thus the

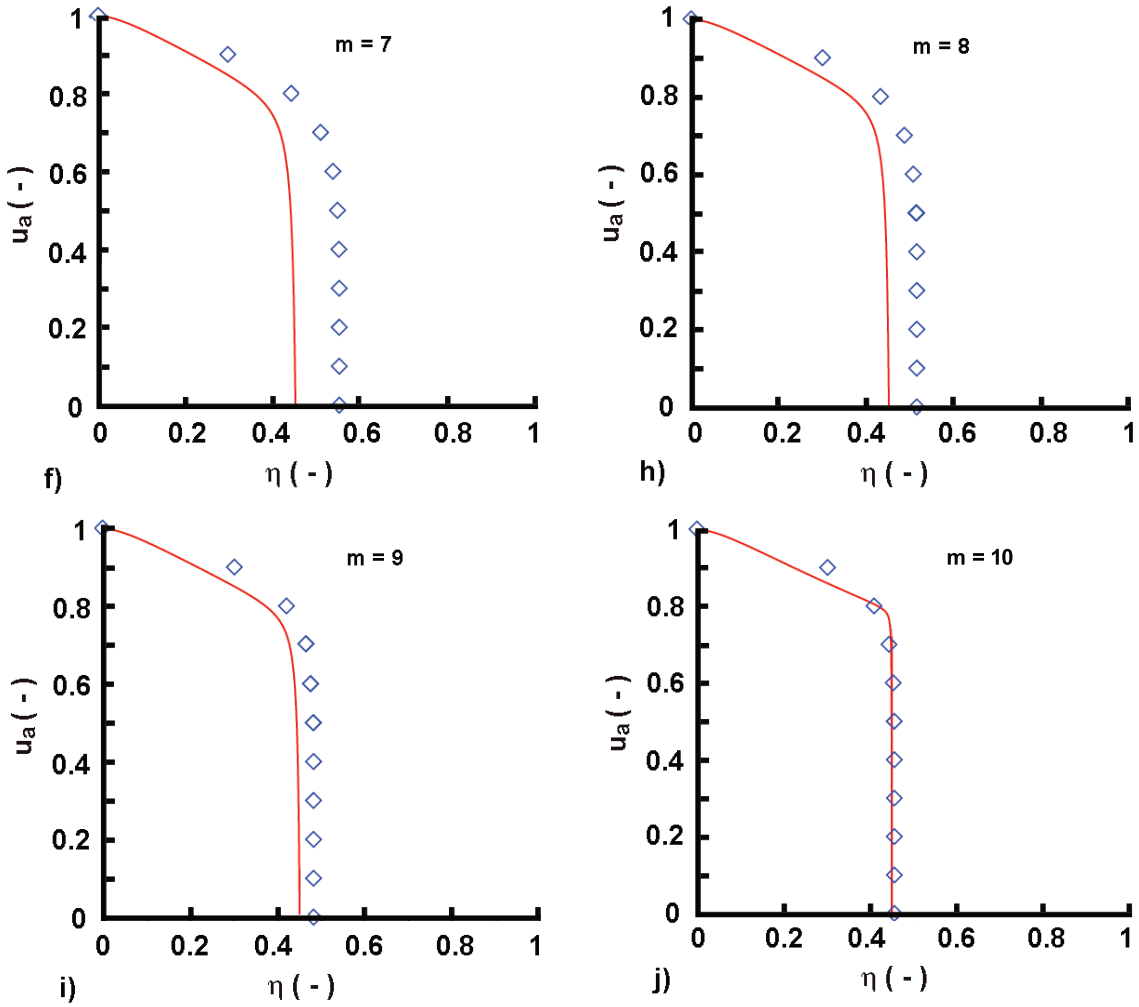

Figure 24. Comparison of the new solution (solid lines) to the numerical results (points) of Parlange et al. [50] for high values of m up to $m = 10$

key point in the new solution is the use of the modified $\sin c(x)$, precisely denoted $\mathrm{Sin}\, c_\pi\,(\pi x^n)$ assumed profile.

- The feature attracting this application as an assumed profile is the possibility of easily controlling its shape by varying the values of the exponent n.
- Especially in the case of the non-linear model solved, the possibility of creating convex profiles for $n > 1$, up to almost rectangular ones for high values of n, is the main attractive point for the solution approach developed.
- The creation of $\mathrm{Sin}\, c_\pi\,(\pi x^n)$ function is also an innovative issue that, to our knowledge, has never been considered before. Its features mentioned at the beginning are only a small group describing its potential, but too many additional ones, beyond the scope of this study, are available and will be outlined in future works.
- The conjecture that the exponent n is dependent on the argument x is also innovative in contrast to the common approach in the integral-balance solutions to determine a fixed optimal value (as in the case of a parabolic profile-based solution [15]).

Some suggestions-1

In the context of envisaged future works, we may draw some points that could be resolved:

- A new assumed profile based on the modified sinc function $\mathrm{Sin}\, c_\pi\,(\pi x^n)$was successfully

applied.

- It was proved that the concept of a variable exponent $n\left(x\right)$ works and allows the modeling concentration profiles with steep fronts corresponding to high values of the non-linearity exponent m.
- The new solution is comparable to the Heaslet Alksne series solution [40] and the integral-balance solution based on a parabolic profile [15].
- The comparative studies indicate that the new solution profiles are almost the same, for high values of the non-linearity exponent m, as the numerical solutions available in the literature.

Some suggestions-2

- Implementation of Sin $c_\pi\left(\pi x^n\right)$ in cases with Neumann, Robin, and time-dependent boundary conditions, for $n>1$, and convex concentration profiles.
- Implementation of Sin $c_\pi\left(\pi x^n\right)$ to cases with other boundary conditions as concave concentration profile for $n<1$.
- Implementation of Sin $c_\pi\left(\pi x^n\right)$ solutions of non-linear models with various non-linear functional relationships of concentration-dependent diffusivity.

In the light of drawn solution problems, it is worth noting that diffusion problems with almost rectangular concentration profiles are of special interest in modeling moisture penetration into concretes [51], soils [52], building materials [53, 53–55], adsorption [56], and some cases of magnetic diffusion [57, 58]. Hence, we can foresee the development of novel implementations of the modified $Sinc_\pi(\pi X^n)$ function in solutions of strong non-linear diffusion problems emerging in various applied fields.

9 Appendices

Derivatives of $Sinc_\pi\left(\pi X^n\right)$ with $n=const.$

Derivatives of $Sinc_\pi\left(\pi X^n\right)$ in terms of trigonometric functions

Denoting for brevity

$$Y\left(X\right)=Sinc_\pi\left(\pi X^n\right)=\sum_{k=0}^{N}\frac{\left(-1\right)^k\pi^{2k}}{\left(2k+1\right)!}X^{2kn}. \tag{53}$$

Then, with $\frac{d}{dt}\left(X\right)=\frac{d}{dt}\left(\frac{x}{\delta}\right)=\frac{x}{\delta^2}\frac{d\delta}{dt}$ we have

$$\frac{d}{dt}Y\left(X\right)=\frac{dY\left(X\right)}{dX}\frac{dX}{dt}=\frac{dY\left(X\right)}{dX}\frac{x}{\delta^2}\frac{d\delta}{dt}, \tag{54}$$

and

$$\frac{d}{dt}Y\left(X^n\right)=\frac{dY\left(X^n\right)}{dX}nX\frac{1}{\delta}\frac{d\delta}{dt}, \tag{55}$$

where

$$\frac{dY\left(X^n\right)}{dX}=\left[\frac{\cos\left(\pi X^n\right)}{X^n}-\frac{\sin\left(\pi X^n\right)}{\pi X^{2n}}\right]nX^{n-1}. \tag{56}$$

For example, with $n = 1$ we have

$$\frac{dY(X)}{dX} = \frac{\cos(\pi X)}{X} - \frac{\sin(\pi X)}{\pi X^2}. \tag{57}$$

Further

$$\frac{d}{dX}[Y(X)]^{m+1} = (m+1)[Y(X)]^m \frac{d}{dX} Y(X), \tag{58}$$

$$\begin{aligned} \frac{d^2}{dX^2}[Y(X^n)]^{m+1} &= \frac{d}{dX}\left[(m+1)[Y(X^n)]^m \frac{d}{dX} Y(X^n)\right] \\ &= m(m+1)[Y(X^n)]^{m-1}\left[\frac{d}{dX} Y(X^n)\right]^2 + (m+1)[Y(X^n)]^m \frac{d^2}{dX^2} Y(X^n). \end{aligned} \tag{59}$$

For example, with $m = 0$ we have

$$\frac{d^2}{dX^2}[Y(X^n)] = \frac{d}{dX}\left[\frac{d}{dX} Y(X^n)\right] = \frac{d}{dX}\left\{\left[\frac{\cos(\pi X^n)}{X^n} - \frac{\sin(\pi X^n)}{\pi X^{2n}}\right] n X^{n-1}\right\}. \tag{60}$$

Derivatives of $Sinc_\pi(\pi X^n)$ as series

As a series the last version of (69) can be presented as

$$\frac{1}{2}\frac{d\delta^2}{dt}\frac{dY(X^n)}{dX} n X^n = \frac{1}{2}\frac{d\delta^2}{dt} n \sum_{k=0}^{N} \frac{(-1)^k \pi^{2k}}{(2k+1)!} X^{2kn} = \frac{1}{2}\frac{d\delta^2}{dt} n \left[\sum_{k=0}^{N} \frac{(-1)^k \pi^{2k}}{(2k+1)!} 2kn X^{2kn-1}\right]. \tag{61}$$

Consequently

$$\frac{d}{dX}[Y(X^n)]^{m+1} = (m+1)[Y(X^n)]^m \frac{d}{dX} Y(X^n) = (m+1)[Y(X^n)]^m n X^{n-1}, \tag{62}$$

and

$$\begin{aligned} \frac{d^2}{dX^2}[Y(X^n)]^{m+1} &= (m+1)\, n \left\{[Y(X^n)]^{m-1} m \frac{dY(X^n)}{dX}(X^n)^2 + \frac{d^2 Y(X^n)}{dX^2}[Y(X^n)]^m\right\} X^{2n-2} \\ &+ [Y(X^n)]^m \frac{dY(X^n)}{dX} X^{2n-2} n(n-1). \end{aligned} \tag{63}$$

As a series $\frac{d^2}{dX^2}[Y(X^n)]$ denoted for the sake of simplicity as Y_{dd} is

$$Y_{dd}(m=0) = \sum_{k=0}^{N} \frac{(-1)^k \pi^{2k} 2kn(2kn-1) X^{2kn-2}}{(2k+1)!}, \tag{64}$$

and when $m \neq 0$

$$Y_{dd}\left(m \neq 0\right) = \left(m+1\right) n^2 \left\{ \begin{array}{l} \left[Y^{m-1}\left(X^n\right) m \dfrac{dY\left(X^n\right)}{dX} \left(X^n\right)^2 + \dfrac{dY\left(X^n\right)}{dX^2} Y^m\left(X^n\right) \right] X^{2n-1} \\ + \left(n-1\right) Y\left(X^n\right) \dfrac{dY\left(X^n\right)}{dX} X^{n-2} \end{array} \right\}. \tag{65}$$

Residual function in case of $n = const.$

Now, we may present the residual function of the approximate solution as

$$R = \frac{\partial}{\partial t} Y\left(X^n\right) - \frac{a_0}{m+1} \frac{\partial^2}{\partial x^2} \left[Y\left(X^n\right) \right]^{m+1}. \tag{66}$$

Changing the spatial variable as $x = X\delta$ we get for the second term:

$$\frac{a_0}{m+1} \frac{\partial^2}{\partial x^2} \left[Y\left(X^n\right) \right]^{m+1} = \frac{a_0}{m+1} \frac{1}{\delta^2} \frac{\partial^2}{\partial X^2} \left[Y\left(X^n\right) \right]^{m+1}. \tag{67}$$

Then,

$$\begin{aligned} R &= \frac{\partial}{\partial t} Y\left(X^n\right) - \frac{a_0}{m+1} \frac{1}{\delta^2} \frac{\partial^2}{\partial X^2} \left[Y\left(X^n\right) \right]^{m+1} \\ &= \frac{1}{\delta^2} \left\{ \left(m+1\right) \delta^2 \frac{\partial}{\partial t} Y\left(X^n\right) - a_0 \frac{\partial^2}{\partial X^2} \left[Y\left(X^n\right) \right]^{m+1} \right\}. \end{aligned} \tag{68}$$

With $\frac{dY(X^n)}{dX} nX \frac{1}{\delta} \frac{d\delta}{dt}$ from (55) and (56) we have after rearrangements

$$\delta^2 \frac{d}{dt} Y\left(X^n\right) = \frac{dY\left(X^n\right)}{dX} nX^{n-1} X\delta \frac{d\delta}{dt} = \frac{1}{2} \frac{d\delta^2}{dt} \frac{dY\left(X^n\right)}{dX} nX^n. \tag{69}$$

This allows to rearrange (68) as

$$R = \frac{a_0}{\delta^2} \left\{ \frac{1}{2} \frac{d\delta^2}{dt} \frac{dY\left(X^n\right)}{dX} nX^n - \frac{\partial^2}{\partial X^2} \left[Y\left(X^n\right) \right]^{m+1} \right\}. \tag{70}$$

Recall, that

$$\delta\left(t\right) = \sqrt{a_0 t} \sqrt{\frac{s_2}{m+1}} \Rightarrow \delta^2\left(t\right) = \frac{a_0 t}{S_2\left(m+1\right)} \Rightarrow \frac{d\delta^2\left(t\right)}{dt} = \frac{a_0}{S_2\left(m+1\right)}. \tag{71}$$

That is, the term $\frac{d\delta^2(t)}{dt}$ is time-independent and contributes as a constant for given n and m. With $\delta^2(t)$ from (71) we get

$$R = \frac{1}{t} \left\{ \frac{1}{2} \frac{dY\left(X^n\right)}{dX} nX^n - S_2\left(m+1\right) \frac{\partial^2}{\partial X^2} \left[Y\left(X^n\right) \right]^{m+1} \right\} = \frac{1}{t} r\left(n, m, X\right). \tag{72}$$

The residual function decays in time and therefore the optimization procedure should address the time-independent term $r\left(n, m, X\right)$. We need $r\left(n, m, X\right) \rightarrow \min$ over the interval $0 \leq X \leq 1$ because for $X = 0$ and $X = 1$ we have $R = 0$, taking into account that $Y\left(1\right) = 0$ and $Y\left(0\right) =$

$1 \rightarrow dY(0)/dX = 0$. The diffusion coefficient a_0 does not affect the minimization of r, now as a function $r(n, X)$ dependent only on the parameter n (for a stipulated m).

Derivatives of $Sinc_\pi(\pi X^n)$ with $n = f(X)$

Derivatives of

$$Y(n(X(x,t))) = \frac{\sin\left(\pi X^{\frac{1}{1-pX(x,t)}}\right)}{\pi X^{\frac{1}{1-pX(x,t)}}}, \tag{73}$$

concerning t and x are

$$\frac{\partial Y}{\partial t} = \frac{p\frac{\partial X(x,t)}{\partial t}\ln(x)}{[1-pX(x,t)]^2}\left[\cos\left(\pi X^{\frac{1}{1-pX(x,t)}}\right) - \frac{\sin\left(\pi X^{\frac{1}{1-pX(x,t)}}\right)}{\pi X^{\frac{1}{1-pX(x,t)}}}\right], \tag{74}$$

$$\frac{\partial Y}{\partial x} = \left(\frac{p\frac{\partial X(x,t)}{\partial x}\ln(x)}{[1-pX(x,t)]^2} + \frac{1}{x[1-pX(x,t)]}\right)\left(\cos\left(\pi X^{\frac{1}{1-pX(x,t)}}\right) - \frac{\sin\left(\pi X^{\frac{1}{1-pX(x,t)}}\right)}{\pi X^{\frac{1}{1-pX(x,t)}}}\right). \tag{75}$$

High-order derivatives, especially $\frac{\partial^2 Y}{\partial x^2}$ and $\frac{\partial^2 Y^{m+1}}{\partial x^2}$ can be easily developed from the above expressions by using computer algebra (such as Maple or others) or by hand. Here we avoid cumbersome expressions that everybody can do.

Declarations

Use of AI tools

The author declares that he has not used Artificial Intelligence (AI) tools in the creation of this article.

Data availability statement

No Data associated with the manuscript.

Ethical approval (optional)

The author states that this research complies with ethical standards. This research does not involve either human participants or animals.

Consent for publication

Not applicable

Conflicts of interest

The author declares that he has no conflict of interest.

Funding

No funding was received for this research.

Author's contributions

This article in all its aspects is a product of the author as follows: Conceptualization, Methodology, Software, Validation, Formal Analysis, Investigation, Resources, Writing - Original Draft, Writing - Review & Editing, Visualization, Supervision.

Acknowledgements

Not applicable

References

[1] Goodman, T.R. The heat-balance integral and its application to problems involving a change of phase. *Transactions of the American Society of Mechanical Engineers*, 80(2), 335-342, (1958). [CrossRef]

[2] Wood, A.S. and Kutluay, S. A heat balance integral model of the thermistor. *International Journal of Heat and Mass Transfer*, 38(10), 1831-1840, (1995). [CrossRef]

[3] Moghtaderi, B., Novozhilov, V., Fletcher, D. and Kent, J.H. An integral model for the transient pyrolysis of solid materials. *Fire and Materials*, 21(1), 7-16, (1997). [CrossRef]

[4] Staggs, J.E.J. Approximate solutions for the pyrolysis of char forming and filled polymers under thermally thick conditions. *Fire and Materials*, 24(6), 305-308, (2000). [CrossRef]

[5] Hristov, J. The heat-balance integral method by a parabolic profile with unspecified exponent: analysis and benchmark exercises. *Thermal Science*, 13(2), 27-48, (2009). [CrossRef]

[6] Hristov J. An approximate analytical (integral-balance) solution to a nonlinear heat diffusion equation. *Thermal Science*, 19(2), 723-733, (2015). [CrossRef]

[7] Bollati, J. and Tarzia, D.A. Approximate solutions to one-phase Stefan-like problems with space-dependent latent heat. *European Journal of Applied Mathematics*, 32(2), 337-369, (2021). [CrossRef]

[8] Canzian, E.P, Santiago, F., Brito Lopes, A.V. and Barañano, A.G. Spherical solidification: An application of the integral methods. *International Journal of Thermal Sciences*, 177, 107575, (2022). [CrossRef]

[9] Canzian, E.P., Santiago, F., Brito Lopes, A.V., Barbosa, M.R. and Barañano, A.G. On the application of the double integral method with quadratic temperature profile for spherical solidification of lead and tin metals. *Applied Thermal Engineering*, 219, 119528, (2023). [CrossRef]

[10] Hristov, J. Multiple integral-balance method: Basic idea and an example with Mullin's model of thermal grooving. *Thermal Science*, 21(3), 1555-1560, (2017). [CrossRef]

[11] Hristov, J. The heat radiation diffusion equation: Explicit analytical solutions by improved integral-balance method. *Thermal Science*, 22(2), 777-788, (2018). [CrossRef]

[12] Bollati, J., Natale, M.F., Semitiel, J.A., Tarzia, D.A. Integral balance methods applied to non-classical Stefan problem. *ArXiv Prints, ArXiv:1810.06370*, (2018). [CrossRef]

[13] Ceretani, A.N., Salva, N.N. and Tarzia, D.A. An exact solution to a Stefan problem with variable thermal conductivity and a Robin boundary condition. *Nonlinear Analysis: Real World Applications*, 40, 243-259, (2018). [CrossRef]

[14] Bollati, J., Natale, M.F., Semitiel, J.A. and Tarzia, D.A. A two-phase Stefan problem with power-type temperature-dependent thermal conductivity. Existence of a solution by two fixed points and numerical results. *AIMS Mathematics*, 9(8), 21189-21211, (2024). [CrossRef]

[15] Hristov J. Integral solutions to transient nonlinear heat (mass) diffusion with a power-law diffusivity: a semi-infinite medium with fixed boundary conditions. *Heat and Mass Transfer*, 52, 635-655, (2016). [CrossRef]

[16] Hill, J.M. Similarity solutions for nonlinear diffusion-a new integration procedure. *Journal of Engineering Mathematics*, 23, 141-155, (1989). [CrossRef]

[17] Smyth, N.F. and Hill, J.M. High-order nonlinear diffusion. *IMA Journal of Applied Mathematics*, 40(2), 73-86, (1988). [CrossRef]

[18] Buckmaster, J. Viscous sheets advancing over dry beds. *Journal of Fluid Mechanics*, 81(4), 735-756, (1977). [CrossRef]

[19] Marino, B.M., Thomas, L.P., Gratton, R., Diez, J.A., Betelú, S. and Gratton, J. Waiting-time solutions of a nonlinear diffusion equation: Experimental study of a creeping flow near a waiting front. *Physical Review E,* 54, 2628, (1996). [CrossRef]

[20] Prasad, S.N. and Salomon, J.B. A new method for analytical solution of a degenerate diffusion equation. *Advances in Water Resources*, 28(10), 1091-1101, (2005). [CrossRef]

[21] Aronson, D.G. The porous medium equation. In: *Nonlinear Diffusion Problems* (pp. 1-46). Springer-Verlag: Berlin, (1986). [CrossRef]

[22] Bradley, D.M. Note on Dirichlet's sinc integral. *The American Mathematical Monthly*, 128(3), 273-274, (2021). [CrossRef]

[23] Stenger, F. Numerical methods based on Whittaker cardinal, or sinc functions. *Siam Review*, 23(2), 165-224, (1981). [CrossRef]

[24] Bercu, G. Sharp bounds on the sinc function via the Fourier series method. *Journal of Mathematical Inequalities*, 13(2), 495-504, (2019). [CrossRef]

[25] Hu, Y. and Mortici, C. A lower bound of the sinc function and its applications. *The Scientific World Journal*, 2014, 571218, (2014). [CrossRef]

[26] Yunlong, W. Sinc sum function and its application on FIR filter design. *Acta Applicandae Mathematicae*, 110, 1037-1056, (2010). [CrossRef]

[27] Gomopoulos, N., Cheng, W., Efremov, M., Nealey, P.F. and Fytas,G. Out-of-plane longitudinal elastic modulus of supported polymer thin films. *Macromolecules*, 42(18), 7164-7167, (2009). [CrossRef]

[28] Abrarov, S.M. and Quine, B.M. A rational approximation of the sinc function based on sampling and the Fourier transforms. *Applied Numerical Mathematics*, 150, 65-75, (2020). [CrossRef]

[29] Stenger, F. *Numerical Methods Based on Sinc and Analytic Functions* (Vol. 20). Springer-Verlag: New York, (1993). [CrossRef]

[30] Morlet, A.C. Convergence of the Sinc method for a fourth-order ordinary differential equation with an application. *SIAM Journal on Numerical Analysis*, 32(5), 1475-1503, (1995). [CrossRef]

[31] Mescia, L., Bia, P. and Caratelli, D. Fractional-calculus-based electromagnetic tool to study pulse propagation in arbitrary dispersive dielectrics. *Physica Status Solidi A*, 216(3), 1800557, (2018). [CrossRef]

[32] Stenger, F. Fourier series for zeta function via Sinc. *Linear Algebra and its Applications*, 429(10), 2636-2639, (2008). [CrossRef]

[33] Cattani, C. Sinc-fractional operator on Shannon wavelet space. *Frontiers in Physics*, 6, 118,

(2018). [CrossRef]

[34] Slavnov, N.A. Integral operators with the generalized sine kernel on the real axis. *Theoretical and Mathematical Physics*, 165, 1262-1274, (2010). [CrossRef]

[35] Yang, X.J., Gao, F., Tenreiro Machado, J.A. and Baleanu, D. A new fractional derivative involving the normalized sinc function without singular kernel. *The European Physical Journal Special Topics*, 226, 3567-3575, (2017). [CrossRef]

[36] Yavuz, M. Characterizations of two different fractional operators without singular kernel. *Mathematical Modelling of Natural Phenomena*, 14(3), 302, (2019). [CrossRef]

[37] Odibat, Z. and Baleanu, D. A new fractional derivative operator with generalized cardinal sine kernel: Numerical simulation. *Mathematics and Computers in Simulation*, 212, 224-233, (2023). [CrossRef]

[38] Odibat, Z., Al-Refai, M. and Baleanu, D. On some properties of generalized cardinal sine kernel fractional operators: Advantages and applications of the extended operators. *Chinese Journal of Physics*, 91, 349-360, (2024). [CrossRef]

[39] Şelariu, M.E., Smarandache, F. and Nitu, M. Cardinal functions and integral functions. *International Journal of Geometry*, 1(1), 27-40,(2012).

[40] Heaslet, M.A. and Alksne, A. Diffusion from a fixed surface with a concentration-dependent coefficient. *Journal of the Society for Industrial and Applied Mathematics*, 9(4), 584-596, (1961). [CrossRef]

[41] Hristov, J. The heat-balance integral: 2. Parabolic profile with a variable exponent: The concept, analysis and numerical experiments. *Comptes Rendus Mécanique*, 340(7), 493-500, (2012). [CrossRef]

[42] Crank, J. *The Mathematics of Diffusion*. Oxford University Press: New York, (1956).

[43] King, J.R. Approximate solutions to a nonlinear diffusion equation. *Journal of Engineering Mathematics*, 22, 53-72, (1988). [CrossRef]

[44] Philip, J. Numerical solution of equations of the diffusion type with diffusivity concentration-dependent. *Transactions of the Faraday Society*, 51, 885-892, (1955). [CrossRef]

[45] Weisberg, L.R. and Blanc, J. Diffusion with interstitial-substitutional equilibrium. Zinc in GaAs. *Physical Review*, 131, 1548, (1963). [CrossRef]

[46] Brutsaert, W. The adaptability of an exact solution to horizontal infiltration. *Water Resources Research*, 4(4), 785-789, (1968). [CrossRef]

[47] Brutsaert, W. A solution for vertical infiltration into a dry porous medium. *Water Resources Research*, 4(5), 1031-1038, (1968). [CrossRef]

[48] Brutsaert, W. and Weisman, R.N. Comparison of solutions of a nonlinear diffusion equation. *Water Resources Research*, 6(2), 642-644, (1970). [CrossRef]

[49] Tuck, B. Some explicit solutions to the non-linear diffusion equation. *Journal of Physics D: Applied Physics*, 9(11), 1559, (1976). [CrossRef]

[50] Parlange, M.B., Prasad, S.N, Parlange, J.-Y. and Römkens, M.J.M. Extension of the Heaslet-Alksne technique to arbitrary soil water diffusivities. *Water Resources Research*, 28(10), 2793-2797, (1992). [CrossRef]

[51] Lockington, D., Parlange, J.Y. and Dux, P. Sorptivity and the estimation of water penetration into unsaturated concrete. *Materials and Structures*, 32, 342-347, (1999). [CrossRef]

[52] Lockington, D. Estimating the sorptivity for a wide range of diffusivity dependence on water content. *Transport in Porous Media*, 10, 95-101, (1993). [CrossRef]

[53] Ioannou, I., Andreou, A., Tsikouras, B., Hatzipanagiotou, K. Application of the sharp front model to capillary absorption in a vuggy limestone. *Engineering Geology*, 105(1-2), 20-23, (2009). [CrossRef]

[54] Küntz, M. and Lavallée, P. Experimental evidence and theoretical analysis of anomalous diffusion during water infiltration in porous building materials. *Journal of Physics D: Applied Physics*, 34(16), 2547, (2001). [CrossRef]

[55] Hristov,J., El-Ganaoui,M. Modelling capillary absorption in building materials with emphasis on the fourth root time law: Time-fractional models, solutions and analysis. In *Fractional Differential Equations: Theoretical Aspects and Applications* (pp. 153-165). Academic Press: New York, (2024). [CrossRef]

[56] Hristov, J. A new closed-form approximate solution to diffusion with quadratic Fujita's nonlinearity: the case of diffusion controlled sorption kinetics relevant to rectangular adsorption isotherms. *Heat and Mass Transfer*, 55, 261-279, (2019). [CrossRef]

[57] Hristov, J. Magnetic field diffusion in ferromagnetic materials: fractional calculus approaches. *An International Journal of Optimization and Control: Theories & Applications*, 11(3), 1-15, (2021). [CrossRef]

[58] Xiao, B., Wang, G., Zhao, L. Feng, C. and Shu, S. An exact solution for the magnetic diffusion problem with a step-function resistivity model. *The European Physical Journal Plus*, 139, 305, (2024). [CrossRef]

Mathematical Modelling and Numerical Simulation with Applications (MMNSA)
(https://dergipark.org.tr/en/pub/mmnsa)

How to cite this article: Hristov, J. (2024). A non-linear diffusion problem with power-law diffusivity: An approximate solution experimenting with a modified sinc function. *Mathematical Modelling and Numerical Simulation with Applications*, 4(5), 6-44. https://doi.org/10.53391/mmnsa.1545438